TURNABLE FABRICATION OF NANOFIBERS POLYVINYLPYRROLYDONE – ZINC OXIDE USING ELECTROSPINING METHOD

Miss Nuchaporn Chewasatn

A Thesis Submitted in Partial Fulfillment of the Requirements

for the Degree of Master of Engineering Program in Chemical Engineering

Department of Chemical Engineering

Faculty of Engineering

Chulalongkorn University

Academic Year 2013

การสังเคราะห์เส้นใยพอลิไวนิลไพโรริโดน-ซิงออกไซด์ที่สามารถปรับแต่งได้โดยการปั่นเส้นใยด้วยไฟฟ้าสถิต

นางสาวนุชาพร ชีวสาธน์

วิทยานิพนธ์นี้เป็นส่วนหนึ่งของการศึกษาตามหลักสูตรปริญญาวิศวกรรมศาสตรมหาบัณฑิต
สาขาวิชาวิศวกรรมเคมี ภาควิชาวิศวกรรมเคมี
คณะวิศวกรรมศาสตร์ จุฬาลงกรณ์มหาวิทยาลัย
ปีการศึกษา 2556

Thesis Title	TURNABLE FABRICATION OF NANOFIBERS POLYVINYLPYRROLYDONE – ZINC OXIDE USING ELECTROSPINING METHOD
By	Miss Nuchaporn Chewasatn
Field of Study	Chemical Engineering
Thesis Advisor	Associate Professor Tawatchai Charinpanitkul, D.Eng.
Thesis Co-advisor	Assistant Professor Varong Pavarajarn, Ph.D.

Accepted by the Faculty of Engineering, Chulalongkorn University in Partial Fulfillment of the Requirements for the Master's Degree

……..… Dean of the Faculty of Engineering
(Professor Bundhit Eua-arporn, Ph.D.)

THESIS COMMITTEE

.....Chairman
(Assistant Professor Anongnat Somwangthanaroj, Ph.D.)

.....Thesis Advisor
(Associate Professor Tawatchai Charinpanitkul, D.Eng.)

…….....Thesis Co-advisor
(Assistant Professor Varong Pavarajarn, Ph.D.)

…….....Examiner
(Assistant Professor Apinan Soottitantawat, D.Eng.)

…….....External Examiner
(Jerawut Kaewsaenee, Ph.D.)

นุชาพร ชีวสาธน์ : การสังเคราะห์เส้นใยพอลิไวนิลไพโรริโดน-ซิงออกไซด์ที่สามารถปรับแต่งได้โดยการปั่นเส้นใยด้วยไฟฟ้าสถิต (TURNABLE FABRICATION OF NANOFIBERS POLYVINYLPYRROLYDONE – ZINC OXIDE USING ELECTROSPINING METHOD) อ. ที่ปรึกษาวิทยานิพนธ์หลัก: รศ.ดร.ธวัชชัย ชรินพาณิชกุล, อ. ที่ปรึกษาวิทยานิพนธ์ร่วม: ผศ.ดร.วรงค์ ปวราจารย์, 90 หน้า.

อนุภาคซิงค์ออกไซด์ในเส้นใยพอลิไวนิลไพโรริโดนสังเคราะห์ได้โดยวิธีการกระจายตัวโดยตรงและการปั่นเส้นใยด้วยไฟฟ้าสถิตย์ โดยการกระจายตัวของอนุภาคซิงค์ออกไซด์ในเส้นใยพอลิไวนิลไพโรริโดนปรับโดยการใช้เทคนิคอัลตร้าโซนิเคท และสารช่วยเพิ่มการกระจายตัว (โซเดียมเฮกซาเมตาฟอสเฟต) ซึ่งพบว่าผลของการใช้เทคนิคอัลตร้าโซนิเคท และสารช่วยเพิ่มการกระจายตัว ช่วยให้อนุภาคของซิงค์ออกไซด์กระจายตัวดีขึ้น เมื่อศึกษาตัวแปรในการปั่นเส้นใยด้วยไฟฟ้าสถิตย์พบว่าผลของค่าศักย์ไฟฟ้าและความเข้มข้นของพอลิไวนิลไพโรริโดนในเอทานอลส่งผลต่อขนาดของเส้นใย และเพื่อทดสอบความคงตัวของเส้นใยที่สังเคราะห์ได้เมื่อโดนแสงยูวี พบว่าเส้นใยพอลิไวนิลไพโรริโดน มีปริมาณพอลิไวนิลไพโรริโดนลดลงถึง 58.14% ในขณะที่เส้นใยพอลิไวนิลไพโรริโดน-ซิงค์ออกไซด์ที่มีการสลายตัวของพอลิเมอร์มากที่สุดมีการสลายตัวสูงกว่า ซึ่งเส้นใยพอลิไวนิลไพโรริโดน-ซิงค์ออกไซด์จะมีความคงทนสูงเมื่อเส้นใยมีปริมาณซิงค์ออกไซด์มากขึ้น โดยผลของสารช่วยกระจายตัวส่งผลให้อัตราการสลายตัวของพอลิไวนิลไพโรริโดนลดลง จากการทดลองเส้นใยพอลิไวนิลไพโรริโดน-ซิงค์ออกไซด์มีการสลายตัวน้อยที่สุดคือเส้นใยที่สังเคราะห์โดยมีปริมาณพอลิไวนิลไพโรริโดนต่อซิงค์ออกไซด์ 5:10 โดยใช้ค่าศักย์ไฟฟ้า13 กิโลโวลต์ และ ปริมาณพอลิไวนิลไพโรริโดน12 เปอร์เซ็นต์โดยน้ำหนักต่อเอทานอล

ภาควิชา วิศวกรรมเคมี ลายมือชื่อนิสิต.....

สาขาวิชา วิศวกรรมเคมี ลายมือชื่อ อ.ที่ปรึกษาวิทยานิพนธ์หลัก.....

ปีการศึกษา 2556 ลายมือชื่อ อ.ที่ปรึกษาวิทยานิพนธ์ร่วม.....

5470251421: MAJOR CHEMICAL ENGINEERING
KEYWORDS: ZnO, PVP, NANOFIBER, ELECTROSPINNING, DIRECT-DISPERSION, STABILITY, DEGRADATION

NUCHAPORN CHEWASATN: TURNABLE FABRICATION OF NANOFIBERS POLYVINYLPYRROLYDONE – ZINC OXIDE USING ELECTROSPINING METHOD. ADVISOR: ASSOC. PROF. TAWATCHAI CHARINPANITKUL, D.Eng., CO-ADVISOR : ASST PROF. VARONG PAVARAJARN, Ph.D., 90 pp.

ZnO particle imbedded in PVP polymer matrix were successfully fabricated by using direct-dispersed processing and electrospinning method. Configuration of PVP-ZnO nanofibers could be manipulated by dispersing ZnO in PVP which is subject to ultrasonication. Effect of ultrasonic dispersion and dispersant on the uniformity of ZnO in PVP matrix showed better microstructure uniformity. The parameters in electrospining process. It was found that the effect of charge density and weight percent of polymer on the electrospun fiber shows an important role on the average fiber diameter. For examination of fibers stability for VOC removal, The fabricated fibers were situated in a photo reactor. The irradiation UV-A could be effective to organic compound and solid-phase PVP degradation. The PVP nanofibers showed the decreasing of 58.14% of the weight of PVP. For the PVP/ZnO fibers degradation, the high ratios of PVP to ZnO fibers showed more stability of fibers than that of the small ratios of PVP to ZnO fibers. And the effect of dispersant on the photocatalytic activity showed that the dispersant on the surface of ZnO particles could decrease photocatalytic activities on catalyst surface. In this study, the most stable fiber was obtained from the PVP/ZnO fibers which were fabricated at the weight ratios of PVP to ZnO 5:10, 13 kV applied voltage, by the 12 weight percent of PVP to Ethanol.

Department : Chemical Engineering Student's Signature .....
Field of Study : Chemical Engineering Advisor's Signature .....
Academic Year : 2013 Co-advisor's Signature .....

ACKNOWLEDGEMENTS

I am very thankful to my thesis advisor and co-advisor, Associate. Professor Dr. Tawatchai Charinpanitkul and Assistant Professor Dr.Varong Panarajarn Department of Chemical Engineering, Chulalongkorn University, who encouraged and gave useful suggestion and discussion through my academic program. Furthermore, I am also thankful to Assistant Professor Dr.Anongnat Somwangthanaroj, Assistant Professor Dr.Apinan Sootitantawat and Dr.Jerawut Kaewsaenee for their comments and participation

This work was partially by Centennial Fund of Chulalongkorn University for the partial financial support to this work.

Furthermore, I would like to thank all members of Center of Excellence in Particle Technology for their help, suggestion and warm collaborations.

Finally, I would like to express my cordial and deep thanks to my family for their love and encouragement.

CONTENTS

PAGE

PAGE

PAGE

PAGE

LIST OF TABLE

Table **PAGE**

LIST OF FIGURES

FIGURE **PAGE**

FIGURE **PAGE**

FIGURE **PAGE**

FIGURE **PAGE**

FIGURE **PAGE**

CHAPTER I

INTRODUCTION

People could expose to air pollutants when they spent most their time indoors, home school and office. Indoor air pollution is one of the major risks to human health. Examples of air pollutant chemicals such as volatile organic compounds (VOCs) would be obtained in the indoor air when it is breathed. Some of these compounds which has been validated by the World Health Organization (WHO) would cause the mucous membrane irritation, headache and fatigue. These symptom are known as sick building syndrome (SBS)[1].

Formaldehyde [2] is listed as a type of VOC in the Eleventh Report on Carcinogens (RoC) and it could reasonably anticipated to be a human carcinogen. Its properties are colorless, flammable, strong-smelling chemical widely used by industries to make home building products. This chemical is generally supplied as a colorless gas type at room temperature, or available as a liquid type called formalin. The United States is a major formaldehyde producer for manufacturing of resins, such as urea-formaldehyde or making the adhesives for wood furniture products. People would incidentally be exposed to formaldehyde in the workplace or in their home environment but the highest risk levels of exposure are found in work settings where formaldehyde is used or produced. The population would accidentally be exposed formaldehyde by breathing tobacco smoke from the indoor or outdoor air. Other combustion sources, such as woodstoves, incinerators, refineries, forest fires, and fumes released from new construction or home-finishing products etc. could produce formaldehyde as VOCs. Other sources, in form of airborne formaldehyde include consumer goods, some hair smoothing and straightening products used in salons, cleaning agents, glues, and adhesive materials.

Elimination of VOCs from indoor air have recently been developed. For examples, the photocatalytic oxidation (PCO) would be a promising approach technology. The air purification technique of PCO principally uses Nano

semiconducting catalysts in association with ultraviolet light to convert organic compounds in indoor air into water vapor (H_2O) and carbon dioxide (CO_2) [3].

Thus photocatalytic degradation using nanosized semiconductors would offer great potentials for the elimination of such VOC. In general, semiconductive metal oxides have been a subject of great research interest due to their size-tunable physicochemical properties, high activities, and non-selective degradability toward various organic pollutants under UV irradiation. Among those metal oxides, zinc oxide (ZnO) with nanostructural properties is a promising substance with a wide direct band gap which could provide many advantages, such as high catalytic activity, more economical cost, environmental friendliness and suitable for various photocatalytic reactions [4-7].

The limitation of use of the nanosized powder with a fluid reactant , e.g. liquid or gas, is of the handling problems, due to the loss of the powder in the fluid stream. Another disadvantage of particulate utilization is the aggregation effect, resulting in a decrease in its surface area [8].

ZnO nanoparticle in the form of nanofiber could be obtained by electrospinning method. This structure still possessed large exposed area of the nanoparticles. Nanofiber was easily handled owing to the extremely high aspect ratios of the products which could reach millimeters in length [8]. Electrospinning is an economical and simple method to prepare fibers with diameters ranging from tens of nanometers to several micrometers. In addition, Nano fiber products could be prepared by other means such as gas–solid reactions, sol–gel methods and direct-dispersed processing [9].

Dispersing nanoparticles directly into the polymer solution prior to spinning is a pathway to fabricate nanofibers. The advantage of this method is the separation of particle. Fiber could also be produced using ZnO nanofibers imbedded in polymer matrix, in particular, the ZnO nanofiber was reported as one of the suitable materials for making VOCs filter. Fabrication of ZnO in PVP matrix was found to result the poor microstructure uniformity. The application of dispersion and ultrasonic mixing could improve the uniformity,

more effectiveness in terms of the size reduction rate, the minimum achievable size, and sedimentation rates [10].

This study is aimed to fabricate the uniform ZnO nanofiber by adjusting on preparing mixture and parameters in electrospining process. This optimization condition could be obtained desired electrospun to use as a filter media which can effectively degrade gas phase of VOCs

This thesis is divided into five chapters. The first chapter describes an introduction and objective of the research. Theory and literature reviews are explained in Chapter II. Chapter III shows materials and the experimental procedure. Chapter IV presents the experimental results and discussion. The final chapter concludes the summary results and gives some recommendation for future works.

CHAPTER II

THEORY AND LITERATURE REVIEWS

This chapter will describe the theory in relation to properties of materials, which are used in this study such as Zinc oxide (ZnO), Polyvinyl pyrrolidone (PVP). The theory and process of the electrospinning will also be described.

2.1 Physical properties of materials used

2.1.1 Physical and chemical properties of Zinc Oxide

Zinc oxide is an inorganic compound with the formula ZnO. Zinc oxide is a white or yellowish powder. There are three crystal structures of ZnO: hexagonal structure like wurtzite, cubic zinc-blende structure and a rarely-observed structure as cubic rock-salt (NaCl-type). Fig.2.1. schematically showed crystal structures of ZnO forms. Under ambient conditions, the thermodynamically stable phase is that of a structure like wurtzite symmetry. The zinc blende ZnO structure can be stabilized when it is growth on cubic substrates, and the rocksalt or Rochelle salt (NaCl) structure may be obtained at relatively high pressures(~2 GPa) [11, 12].

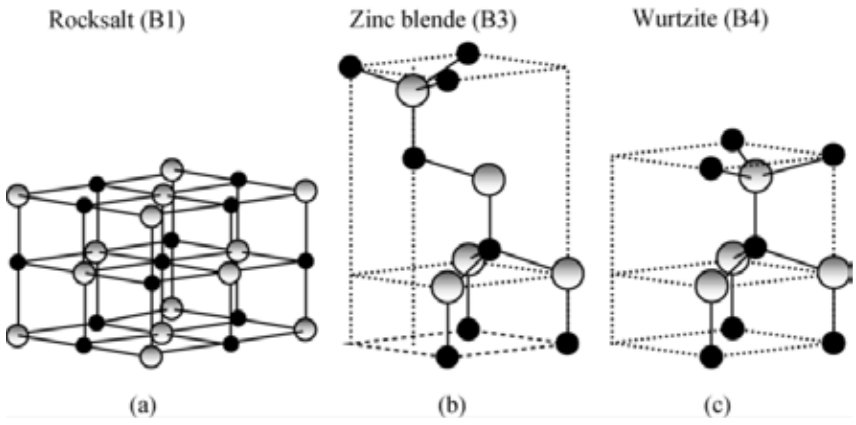

Fig 2.1 Stick-and-ball representation of ZnO crystal structures :(a) cubic rocksalt (B1), (b) cubic zinc blende (B3), and (c) hexagonal wurtzite (B4). Shaded gray and black spheres denote Zn and O atoms, respectively.

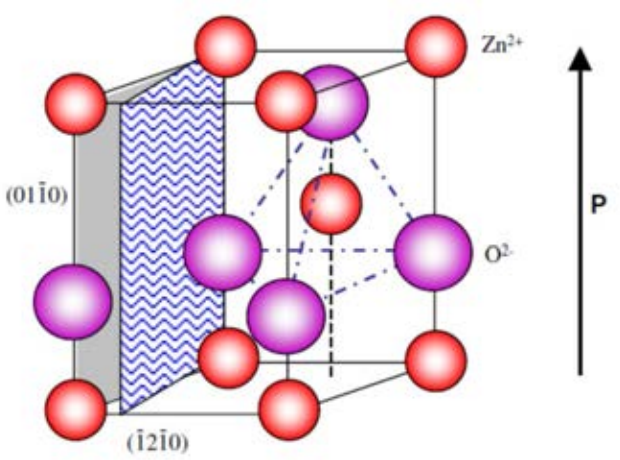

Fig.2.2. The wurtzite structure model of ZnO. The tetrahedral coordination of Zn–O.

Wurtzite zinc oxide can found in a form of a hexagonal structure with lattice parameters a = 0.3296 and c = 0.520 65 nm. The structure of ZnO can be simply described as a number of alternating planes composed of tetrahedrally coordinatedO_2^- and Zn_2^+ ions, stacked alternately along the c-axis (Fig.2.2). The tetrahedral coordination in ZnO results in noncentral symmetric structure. Another important characteristic of ZnO is polar surfaces.

Zinc oxide is an n-type semiconductor with a band gap of 3.20 eV and the free excitation energy of 60 meV. This excitation energy makes ZnO very high potential for room temperature light emission. Zinc oxide also has strong resistance to high temperature electronic degradation during operation. Its high refractive index (1.95–2.10) was useful in pigment applications and it can be an electrical conductor when a suitable dopant type and does is in traduced. Another property is thermally stable to extremely high temperatures (at least ~1800 °C). The physical and chemical properties of ZnO powder ensure a large off-take as an additive in rubber. Alternatively, the high specific surface area of the 'active' grades permits them to be used in desulfurization processes in chemical plants. In addition, it is attractive for many opto-electronic applications in the range of blue and violet light as well as UV devices for wide range of technological applications**.** Zinc oxide also exhibits dual semiconducting and piezoelectric properties [12]. The other properties are given in Table 2.1

Table 2.1 Properties of wurtzite zinc oxide.

Molecular formula	ZnO
Molecular weight	81.38 g/mole
Lattice parameters at 300 K:	
A	0.32495 nm
C	0.52069 nm
a/c	1.602 (ideal hexagonal structure is 1.633)
Relative dielectric constant	8.66
Density	5.606 g/cm^3
Melting point	1970 – 1975 °C (decomposes)
Thermal conductivity	130 W/m.K
Electron effective mass	0.24
Electron mobility (T = 300 K)	200cm^3/Vs
Intrinsic carrier concentration	< 106 cm^{-3}
Static dielectric constant	8.656
Hole effective mass	0.59
Hole mobility (T = 300 K)	5-50 cm^2/Vs
Energy gap	3.2 eV, direct
Excitation binding energy	60 meV
Appearance	White solid
Synonyms	Zinc white; Zinc flowers; Calamine; C.I. pigment white 4
Solubility	Insoluble in water and alcohols. Soluble in acids and bases.
Physicochemical stability	Stable under normal conditions of handling and storage.

2.1.2 Polymers

Poly vinyl pyrrolidone (PVP) is a thermoplastic having linear Formula $(C_6H_9NO)_n$ as showed in Fig 2.3. High molecular weight PVP have been used as a polymer media to increase the viscosity of the solution in many work, in particular, electrospinning process. PVP can be dissolved in polar solvents such as water and

ethanol. Watthanaarun et al. (2005) [13] used this PVP material to produce nanofiber. But Giri et al. (2011) [14] use PVP material as a binder for formation of nano silver particles, which would be applied in medical field. PVP is a water soluble polymer with a large number of consumer uses. This commercial success derives from its biological compatibility, low toxicity, film-forming and adhesive characteristics, unusual complexing ability, relatively inert behavior toward salts and acids, and its resistance to thermal degradation in solution.

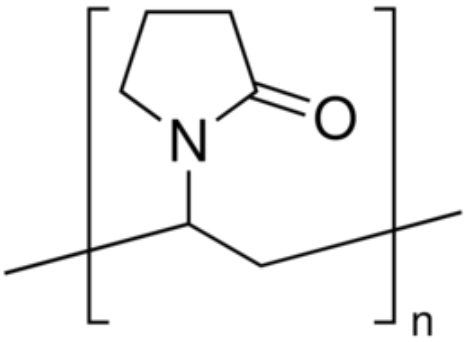

Fig.2.3 The structural formular of Poly vinyl pyrolydone

2.1.3 Dispersant

Sodium hexametaphosphate (SHMP) is a hexamer of composition $(NaPO_3)_6$ as shown in Fig 2.4. Sodium hexametaphosphate has applications in a wide variety of industries, including as a food additive. Sodium carbonate is sometimes added to SHMP to raise the pH to 8.0-8.6 for production of a number of SHMP products which are used for water softening and detergents. This chemical can be used as a dispersing agent to break down clay and other soil types. They are more commonly used in laboratory procedures to sustain suspensions and estimate particle size distribution.

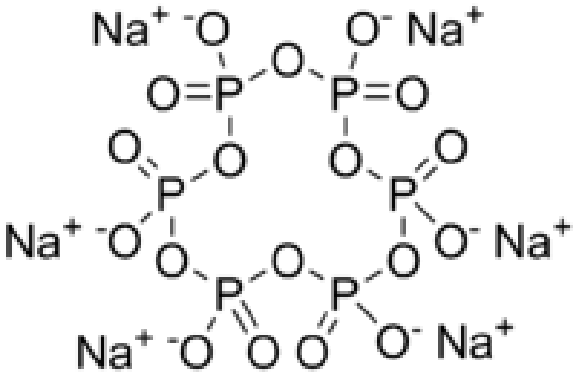

Fig.2.4 The structural formular of Sodium hexametaphosphate

Park et al (2009) [15] use five different dispersants to treat the synthesized ZnO nanopowders. Their dispersion characteristics were analyzed through mobility and zeta potential. Sodium hexametaphosphate is the most effective dispersant. Dispersion of photocatalyst powders is required to prevent the flocculation of the powders. The dispersion can be achieved by separating photocatalyst powders from each other. This result could be obtained by making the powder surface positively charged or negatively charged. Cation or anion could be easily adsorbed on powder surface. Then the charged powders repulse each other and eventually lead to larger surface area for photocatalytic reactions.

2.2 Electrospining process

2.2.1 Electrospinning technique

Electrospinning [16] is a broadly used technology for electrostatic fiber formation. This technique utilizes natural or synthetic polymer solution in association with electrical forces to produce polymer fibers with diameters ranging from 2 nm to several micrometers. Both natural and synthetic polymers have presented a tremendous increase in research and commercial attention over the past decade.

This process of electrospinning has gained much attention in the last decade not only due to its versatility in spinning a wide variety of polymeric fibers but also due to its ability to consistently produce fibers in the submicron range consistently that is otherwise difficult to achieve by using standard mechanical fiber-spinning

technologies techniques [17]. With smaller pores and higher surface area than regular fibers, electrospun fibers have been successfully applied in various fields, such as, nanocatalysis, tissue engineering scaffolds, protective clothing, filtration, biomedical, pharmaceutical, optical electronics, healthcare, biotechnology, defense and security, and environmental engineering

Electrospinning, a spinning technique, is a unique approach using electro static forces to produce fine fibers from polymer solutions or melts and the resulting fibers have a thinner diameter and a larger surface area than those obtained from conventional spinning processes. Furthermore, a DC voltage in the range of several tens of kVs is necessary to be generated for the electrospinning. Various techniques such as electrostatic precipitators and pesticide sprayers work are similar to the electrospinning process and this process, mainly based on the principle that strong mutual electrical repulsive forces overcome weaker forces of surface tension in the charged polymer liquid [18].

There are two standard electrospinning setups, vertical and horizontal. With the expansion of this technology, several research groups have developed more sophisticated systems that can fabricate more complex nanofibrous structures in a more controlled and efficient manner [19, 20]. Electrospinning is conducted at room temperature with atmosphere conditions. The typical set up of electrospinning apparatus is shown in Fig. 2.5 (a and b). Basically, an electrospinning system consists of three major components: a high voltage power supply, a spinneret (e.g., a pipette tip) and a grounded collecting plate (usually a metal screen, plate, or rotating mandrel) and utilizes a high voltage source to inject charge of a certain polarity into a polymer solution or melt, which is then accelerated towards a collector of opposite polarity. Most of the polymers are dissolved in some solvents before electrospinning, and when it completely dissolves, forms polymer solution. The polymer fluid is then introduced into the capillary tube for electrospinning [21].

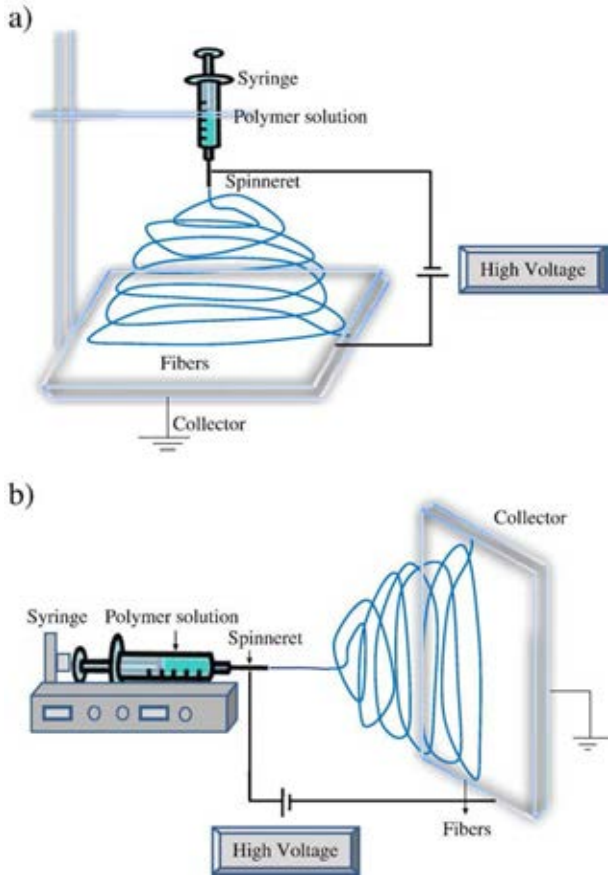

Fig. 2.5 Schematic diagram of set up of electrospinning apparatus (a) typical vertical set up and (b) horizontal set up of electrospinning apparatus [21].

In a prototypical electrospinning experiment, a jet path was created when a fluid polymer solution, supplied to a drop attached to an orifice by surface tension and viscoelastic stresses, was electrified by a sufficiently large electrical potential applied between the drop and a collector some distance away. The shape of the drop approached a cone and an electrically charged jet of fluid emanated from the tip of the cone. The jet followed a path that began with a straight segment. The diameter of the jet, in the straight segment, decreased monotonically with distance from the tip. Each segment of the jet retained most of its downward velocity, but surprisingly, moved radially outward at a comparable velocity as the electrical bending instability developed. Electrical forces from the charge carried with the jet caused the jet to continue to elongate as it coiled. The thin fluid jet finally solidified into a nanofiber as shown in Fig 2.6 [16, 22, 23].

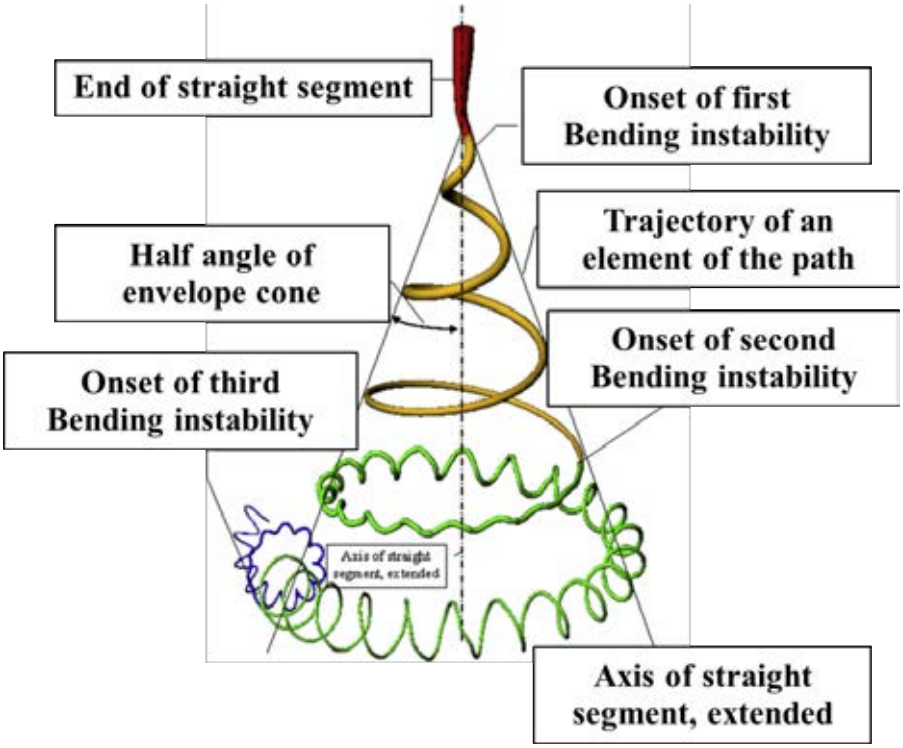

Fig. 2.6 Schematic diagram of electrospinning jet [16].

Interactions of polymer molecules in the fluid and the electrical forces from excess ions carried with the jet generally prevented the onset of the capillary instability. Sometimes the capillary instability occurred, and converted the cylindrical jet to a series of droplets which solidified into beads supported on a nanofiber.

2.2.2 Parameter Investigation

Many parameters can influence the transformation of polymer solutions into nanofibers through electrospinning such as the polymer (type, molecular weight), solvent (types, vapor pressure, diffusivity in air), additives (surfactants, salts), polymer concentration, solution properties (rheological behavior, relaxation time, viscosity, surface tension, electric conductivity and dielectric permittivity), electric field (strength, geometry), solution feed rate, nozzle orifice diameter, distance from nozzle to collector, and ambient conditions (relative humidity, temperature, etc.). Most viscosity values which are measured and reported are zero-shear values. Nearly every referenced work concluded that when electrospinning solution is increased to

zero-shear viscosity, a higher MW polymer or higher concentration will increase the resulting fiber radius [24].

Yun et al. (2007) [25] prepared Polyacrylonitrile (PAN) fibers by electro-spinning for use as a filter media. When these PAN fibers were compared to commercial filters made of polyolefin and glass, the fibers of electrospun filters were more uniform in diameter. The performance of electrospun filters was evaluated by measuring the penetration of monodisperse NaCl nanoparticles (below 80 nm) through the filters. It was found that electrospun filters could be made which had nanoparticle penetration values comparable to commercial filters but it is substantially less filter mass. Electrospinning allows for advanced fibrous materials production with controlled, uniform fiber size which allows for the production of low nanoparticle penetration, low mass filters (Fig 2.7). [26].

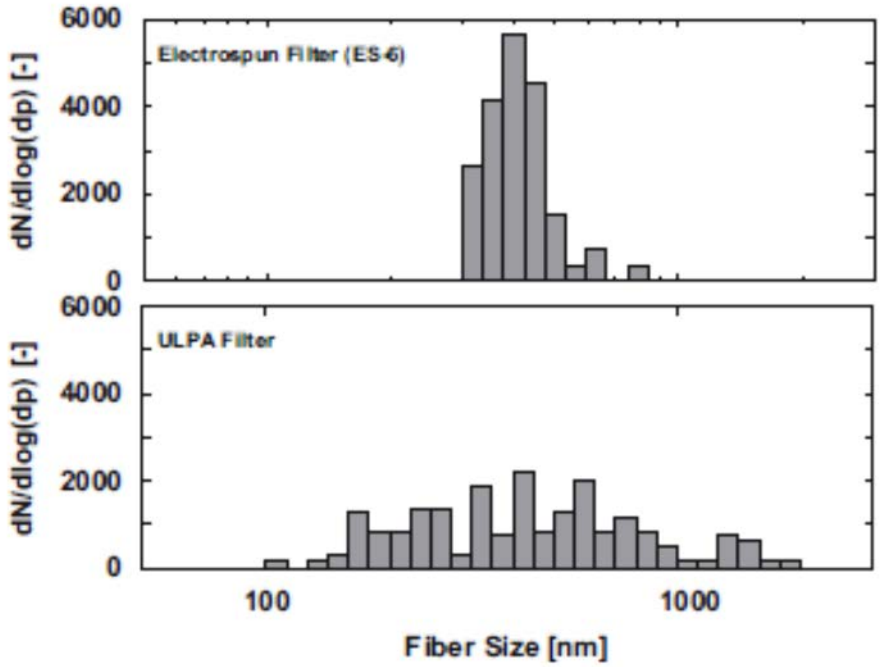

Fig. 2.7. Fiber diameter distributions of commercial and electrospun filter fibers [25].

Electrospinning exhibited the unique ability to produce diverse forms of fibrous assemblies. The remarkable specific surface area and high porosity bring electrospun nanomaterials highly attractive in nanotechnological applications. The applications of the electrospun nanomaterials was reported.

Park et al. (2009) [15] fabricated ZnO nanofibers by combining sol–gel process and electrospinning method for identifying CO gas sensing capacity. The crystallinity of ZnO nanofibers improved with increase in annealing temperature. The diameters of fully crystalline ZnO nanofibers after annealing above 600^{o}C ranged from 35 nm to 100 nm. The ZnO nanofibers showed CO gas sensing capacity at concentration as low as 1.9 ppm.

Sangkhaprom et al. (2010) [8] synthesized ZnO nanostructure in a form of beaded fibers by combined electrospinning and solvothermal techniques. It was found that zinc acetate within the PVA matrix was converted into ZnO nanoparticles in hexagonal structure like wurtzite structure, while PVA was still retained within the structure. Therefore, the product was no longer easy to crumble into powder and easy to handle. Size of the ZnO particles and a diameter of the product depends upon the concentration of zinc acetate within the precursor fibers as showed in Fig.2.8

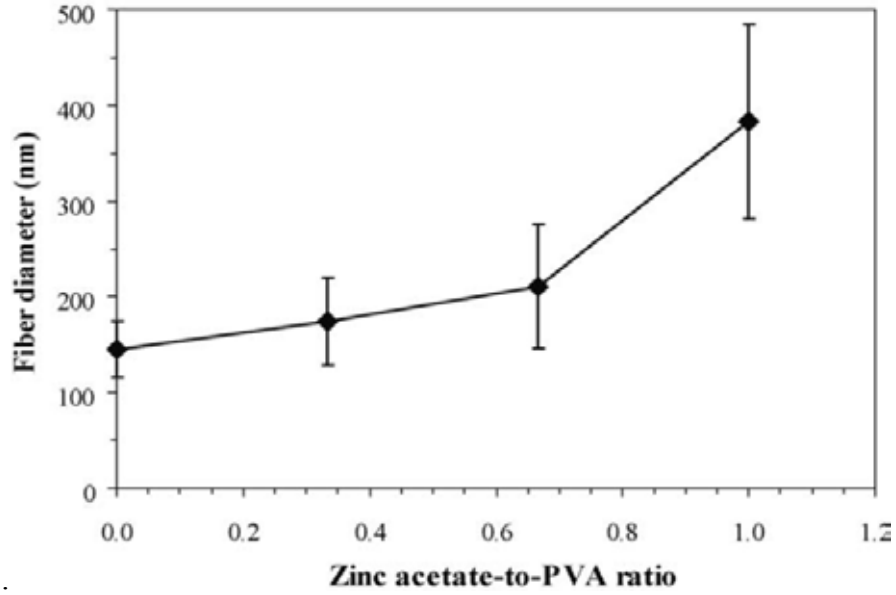

Fig. 2.8. Diameters of as-spun precursor fibers as a function of zinc acetate content. The error bars in the figure represent standard deviation of the fiber diameter data [8].

Watthanaarun et al (2005) [13] produced polyvinylpyrrolidone (PVP) / Titanium (IV) oxide composite nanofibers by Sol–gel and electrospinning techniques.

Diameters of the obtained composite fibers were in the range of 120–350 nm. The effects of PVP concentration and electrostatic field strength on size and size distribution of the as-spun fibers were investigated in Fig 2.9.

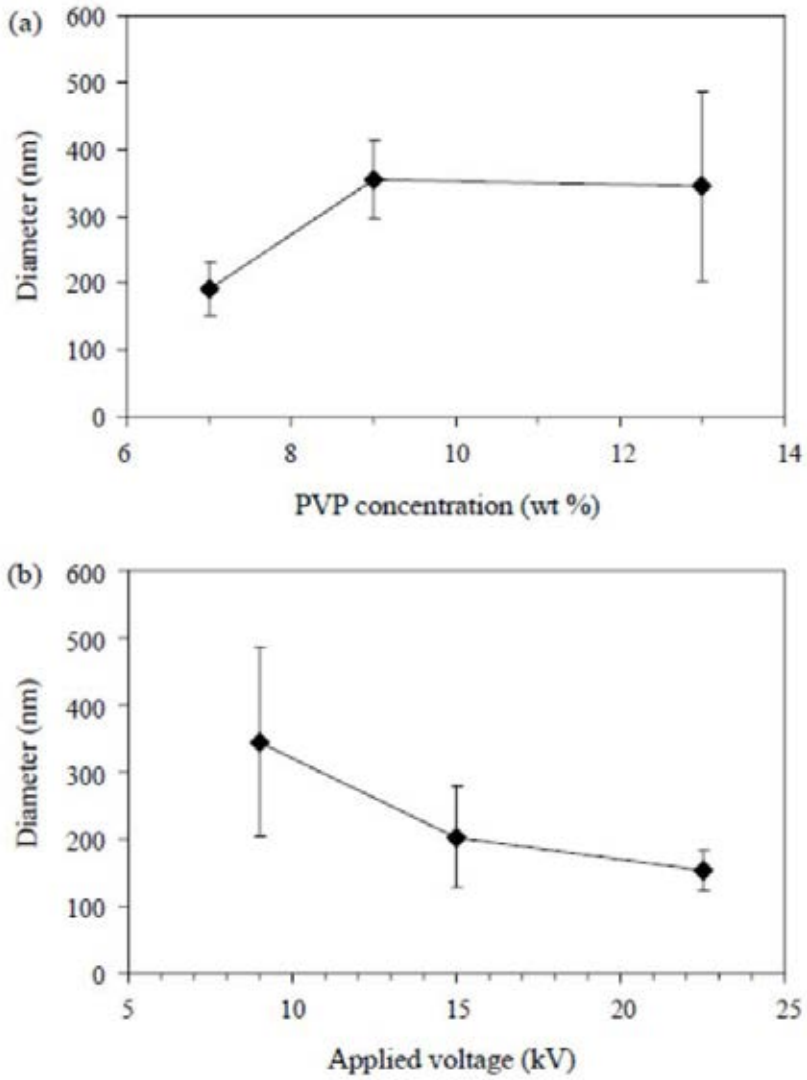

Fig.2.9. Diameters of pre-calcined as-spun fibers as a function of (a) PVP concentration and (b) applied electrostatic potential [13].

2.2.3 The preparation of electrospinning solution by Direct dispersion method

Various means have been combined with electrospinning, such as gas–solid reactions, sol–gel methods and direct-dispersed processing to prepare composite nanofibers. Dispersing nanoparticles directly into the polymer solution prior to spinning is an obvious pathway to fabricate composite nanofibers. The advantage of

this method is the separation of particle synthesis and electrospinning process to obtain specific composite nanofibers with a wide range of properties [27].

To insert an inorganic nanocomponent into a polymer fiber, the most straightforward strategy is to disperse the inorganic nanocomponents in a polymer solution, and followed by electrospining. However, the inorganic nanocomponents were easily aggregated in polymer fibers. Zhang et al. (2010) [28] tired to make silver nanoparticles in PAN fibers using directed dispersion method. The transmission electron microscopy (TEM) studies shows that the silver nanoparticles had partially aggregated. To make the inorganic nanoparticles effectively disperse in polymer nanofibers, sometimes a surfactant is needed. Wang et al. (2007) [29] studied the dispersion of CdTe quantum dot (QDs) in PVP solid nanofibers by the direct dispersed electrospining method. The CdTe QDs congregated in the PVP fibers after electrospining in the absence of cetyltrimethylammonium bromide (CTAB). In contrast, CdTe QDs could be well dispersed in the PVP fibers after adding a small amount of CTAB.

He et al (2003) [30] fabricate PVA–Pt/TiO_2 composite nanofiber aggregate by direct dispersion and electrospinning method and investigate the photocatalytic degradation of solid-phase PVA. as shown in Fig 2.10

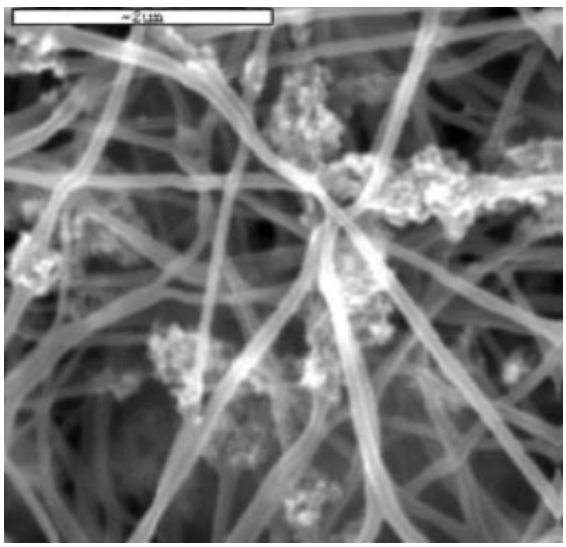

Fig.2.10 SEM image of PVA–Pt/TiO_2 composite nanofiber [30].

2.2.4 Ultrasonication method

Due to the individual particles are held together by attraction force such as van der waals forces and liquid surface tension. Chung et al.(2009) [10] studied the suspensions of ZnO nanoparticles in water with a two-step powder dispersion process using several methods of ultrasonication. It has been found that dispersion of ZnO from two different commercial suppliers appears to proceed by fragmentation rather than erosion of individual particulates, with a minimum particulate size of 50–300 nm, arranged in compact aggregates. Dispersion by ultrasonic horn is found to be more effective in terms of the size reductionrate, the minimum achievable size, and sedimentation rates.

In an ultrasonic system, the sidewalls of a bath or end of a horn were driven at ultrasonic frequencies by piezo transducers or solenoids to induce oscillations (typically 20–50 kHz). Energy is transferred into the fluid in the form of pressure waves that induce cavitation that subsequently is forced to collapse, and releases intense pressure waves into the surrounding fluid. Particles adjacent to the cavity are subjected to normal and shear forces which can cause breakage of the particle if they are of sufficient intensity [10].

2.3 The photodegradation of Polymer

Photo-oxidative degradation is the process of decomposition of the material by the action of light, which is considered as one of the primary sources of damage exerted upon polymeric substrates at ambient conditions. Most of the synthetic polymers are susceptible to degradation initiated by UV and visible light [31]. Polymer degradation occurs mainly in the ether parts of the soft-segments, where photo-irradiation generates ester, aldehyde, formate and propyl end groups **.** UV radiations have sufficient energy to cleave C-C bond [32]. Photodegradation changes the physical and optical properties of the plastic. The most damaging effects are the visual effect (yellowing), the loss of mechanical properties of the polymers, the changes in molecular weight and the molecular weight distribution for the same . PE and PP films when exposed to solar UV radiation readily lose their extensibility,

mechanical integrity and strength along with decrease in their average molecular weight [33, 34].

Gijsman et al.(1999) [17] presented the photodegradation mechanism of polymers highly depends on the type and concentration of chromophores. This influence was studied by making a comparison between the UV-degradation of PE, PP, PA6 and PBT and the thermooxidative degradation of PP at a comparable temperature. The degradation processess were followed by determining the oxygen uptake, CO, CO_2 and peroxide formation. Thickness degradation profiles showed that the UV- degradation processes of PP and PBT were heterogeneous. PP degradation would be caused by oxygen diffusion limit where as PBT degradation was the result of absorption of the UV light.

All polymers degradation rate depends on the environment, especially sunlight intensity, temperature and humidity and the type of polymer. UV-degradation would combine effects of photolysis and oxidative reactions. In an inert atmosphere, only the photolysis process is active and in the presence of air, photooxidation could be an important key for degradation process. Sunlight photolytic degradation and/or photooxidation can only occur when the polymer contains chromophores which absorb wavelengths of the sunlight spectrum on earth. These wavelengths have sufficient energy to cause a dissociative (cleavage) process, resulting in degradation. According to the law of Lambert-Beer, the absorption of light (A) is related to the extinction coefficient of the absorbing chromophores (E), the concentration of these groups (C) and the thickness of the sample (T) (A=E. C. T). Chromophores that can absorb sunlight are:

- Internal in-chain impurities such as hydroperoxides or carbonyls formed during storage, processing or weathering.
- External impurities as polymerisation catalyst residues, additives (e.g. pigments, dyes or antioxidants), pollutants from the atmosphere or metal traces from processing equipment.
- Parts of the molecular structure of the polymer.
- Charge transfer complexes between oxygen and the polymer chain.

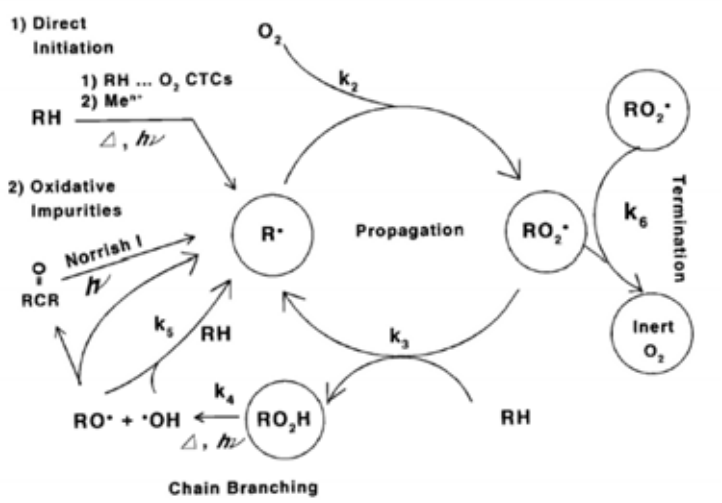

Fig. 2.11 Autooxidation mechanism for almost all polymers (R=polymer chain, H=most labile hydrogen, X^o, any radical, k_i=reaction rate) [17].

In the presence of air, almost polymers degrade faster than in an inert environment. This type of degradation is called photooxidative degradation. Photooxidative degradation is due to a radical-based autooxidative process as showed Fig 2.11

2.3.1 Mechanism of photodegradation

The mechanisms of the degradation and oxidation reactions are determined by the extraneous groups and/or impurities in the polymer, which absorb light quanta and form excited states. Initially short-lived singlet state is transformed to long-lived triplet state [35]. Excited triplet states may cleave the polymer chains and form radical pairs (Norrish Type I reaction) or form pairs of saturated and unsaturated chain ends by hydrogen transfer (Norrish Type II reaction) [36]. The polymer radicals thus formed may add molecular oxygen (in triplet ground state) to peroxy radicals, which abstract hydrogen and form hydroperoxide groups, which absorb UV light or become excited by energy transfer, the weak O-O bonds break and pairs of alkoxy and hydroxyl radicals are formed which may react in various ways, e.g. by hydrogen abstraction, chain scission, rearrangement, etc. and accelerate photodegradation [37]. Double bonds may add excited oxygen molecules in singlet state. In this reaction, the double bond is shifted to an adjacent C-C bond and a

hydroperoxide group is formed. Some synthetic polymers, e.g. aromatic polyesters and polyamides, have inherent absorption of UV light, causing excitation, radical formation, oxygen addition, splitting off small molecules, chain scission, etc. Some of these polymers are auto-stabilized towards photodegradation by formation of an oxidized surface layer with high absorption of near UV and visible light of short wavelengths, preventing further penetration of light into deeper layers [38]. In photo-oxidative degradation, mechanism involves autooxidation cycle comprising various steps.

2.3.1.1 Initiation

The absorption of UV light that has sufficient energy to break the chemical bonds in the main polymerchain leads to the initiation of mechanism responsible for polymer degradation. It involves a radical chain mechanism for the formation of initial radical. Different initiation steps under varied conditions have been undertaken in different polymers.

2.3.1.1.1 Direct UV initiated photolysis of C-C and C-H bond.

Bond dissociation energy of C-C bond (375 kJ/mol) and C-H bond (420 kJ/mol) is equivalent to UV radiation of 320 nm and 290 nm. Thus, direct photolysis of C-C and C-H bond is possible and the radical formed in these reactions become a source of initiation radicals as shown in Fig.2.12[31].

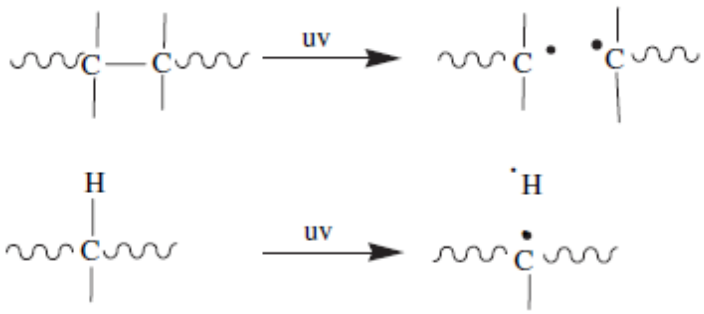

Fig. 2.12 Schematic of direct UV initiated photolysis of C-C and C-H bond[39] .

2.3.1.1.2 Photosensitized cleavage.

Photosensitizers are highly photosensitive, readily get excited on exposure to light and are generally employed to bring about effective hemolysis of the polymeric chains, which otherwise do not undergo sufficient photo-excitation at the frequency of light available to the system as Fig 2.13

Fig.2.13 Schematic of Photosensitized cleavage.

2.3.1.1.3. Catalyst residues as source of generation of radicals.

Some metal salts and oxidation products of such residues when added to the polymers act as catalysts to generate initiation radicals as Fig 2.14 [40]. Polymerization catalysts such as transition metals (Ti) may remain in polyolefins at 2-100 ppm, depending on workup and catalyst efficiency. These residues have been implicated in both photo- and thermal stability problems. For example, TiO2 is a well-known photosensitizer for polyamide and polyolefin degradation and absorbs at 480 nm. Photosensitization involves the formation of highly reactive species including atomic oxygen, $^{\cdot}OH$, $^{\cdot}OOH$ and $O^{\cdot}_2$. The primary process involves the promotion of the Ti electron to the conduction band of the semiconductor to form an electron-positive hole pair. The relative proportions of the reactive species depend on the presence of water. No TiO2 sensitization will be observed unless both oxygen and water are present [32].

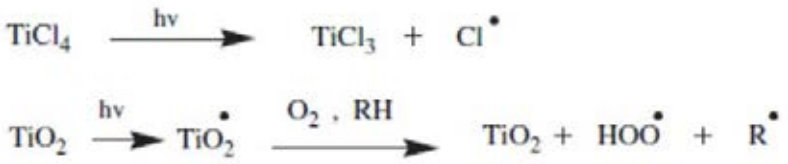

Fig. 2.14 Schematic of catalyst residues as source of generation of radicals.

2.3.1.1.4. Incorporation of carbonyl groups.

Carbonyl groups formed by mild oxidation of polymer during synthesis or processing act as chromophores and become source of the initiation radicals. Carbonyl chromophore absorbs near-UV radiations and subsequently forms radicals following Norrish Type I, Norrish Type II and H-atom abstraction processes as Fig.2.15 [41].

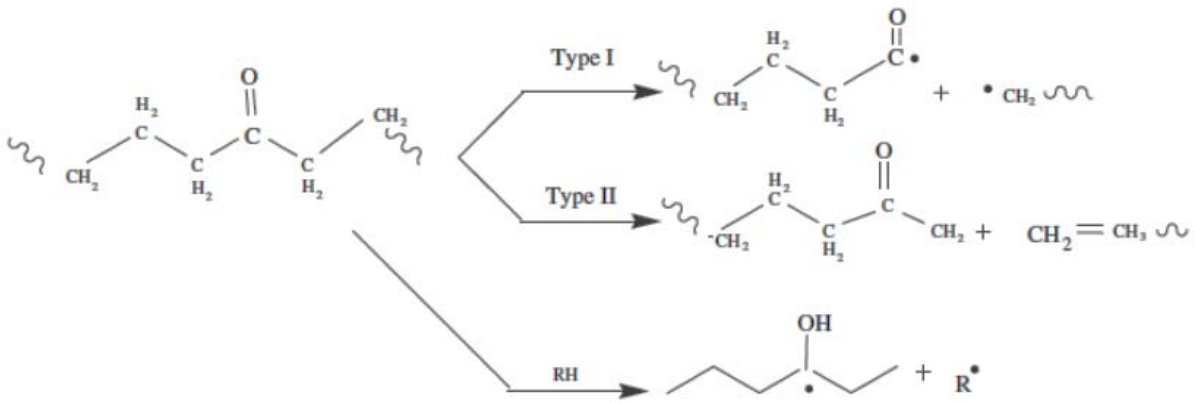

Fig. 2.15 Schematic of Incorporation of carbonyl groups [41] .

2.3.1.1.5. Introduction of peroxides or site of unsaturation.

The peroxides or C=C sites become source of initiation radicals. The near UV component of sunlight is energetic enough to cleave C-C bond provided that light of the appropriate wavelength is absorbed. Chain oxidation occurs in most of the polymers because of the labile O-O bond present in the macrohydroperoxide –C-OOH, the macroalkoxyl and hydroxyl radicals thus formed may abstract hydrogen from the surrounding polymer matrix to generate alcohol, water and new macroalkyl radicals which can then take part in many cycles of the chain-initiation reactions. In the case of unsaturated polymers, light generated singlet oxygen $^1O2$ reacts with an

unsaturated site by way of an ‘‘ene’’ reaction and starts chain oxidation as Fig. 2.16 [32].

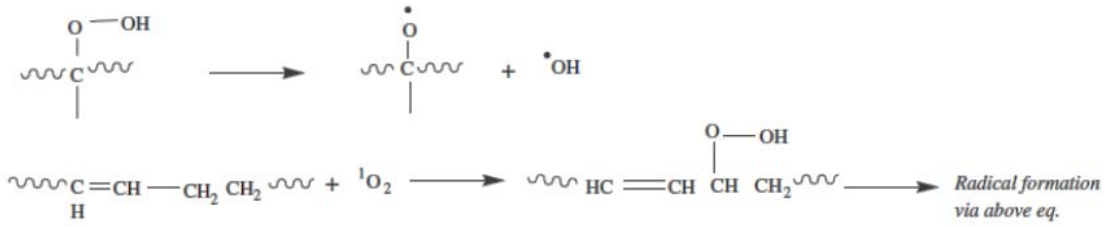

Fig.2.16 Schematic of introduction of peroxides or site of unsaturation [32].

2.3.1.1.6. Reactions of singlet and triplet stage.

Reaction of a ketone in a triplet-excited state with ground state oxygen is another potential initiation reaction as Fig 2.17. In these reactions, UV light is absorbed by carbonyl or other chromophoric groups and the energy of the excited groups is transferred to oxygen molecules. The resulting excited oxygen species react with vinyl or other unsaturated groups forming hydroperoxide which then initiate free radical reaction mechanism [35].

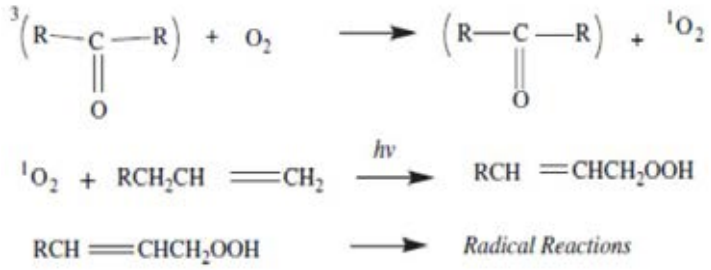

Fig.2.17 Schematic of reactions of singlet and triplet stage [35].

2.3.1.2. Propagation reaction

The propagation reactions are thermal reactions. The rate of the reaction of oxygen with alkyl radicals is very high [42] and that is why the rate of the propagation is largely determined by the ease of hydrogen abstraction in the second step of the propagation. Photochemically, hydroperoxides can decompose homolytically into alkoxy and hydroxy radicals [43, 44],which can initiate an other propagation cycle. The quantum yield of this reaction is very high. E.g. For Polyethylene, it has been shown that the hydroperoxidesformed during a

thermooxidative degradation do not initiate the photooxidation [45-47]. Several hydroperoxide decomposition mechanisms have been proposed, some of which lead to radicals and/or chain scission and others do not [48, 49].

2.3.1.3 Terminal reaction

Termination reactions are bimolecular. In the presence of sufficient air, which is normally the case for the long-term degradation of polymers, only the reaction of two peroxy radicals has to be considered [50]. The reaction depends on the type of peroxy radical present. For tertiary peroxy radicals (as present in PP) the termination reaction leads to dialkylperoxides, while secondary peroxy radicals (as formed in PE, PA6 and PBT) can react according to the Russell mechanism, resulting in an alcohol and a ketone [51].

2.4 The Photocatalytic degradation

The air purification technique of PCO commonly uses nano semiconductor catalysts and ultraviolet (UV) light to convert organic compounds in indoor air into water vapor (H_2O) and carbon dioxide (CO_2) [3] . Fig.2.18 shows the schematic of the UV-PCO process of VOCs using TiO_2 as the catalyst. An electron in an electron-filled valence band (VB) is excited by photo irradiation to a vacant conduction band (CB), leaving a positive hole in the VB. These electrons and positive holes drive reduction and oxidation, respectively, of compounds adsorbed on the surface of a photocatalyst [52].

The activation equation can be written as:

$$TiO_2 + hv \rightarrow h^+ + e^-$$

In this reaction, h+ and e- are powerful oxidizing and reducing agents, respectively. The oxidation and reduction reactions can be expressed as:

Oxidation reaction : $h^+ + OH^- \rightarrow OH^-$

Reduction reaction : $e^- + O_{2ads} \rightarrow O^-_{2ads}$

When organic compounds are chemically transformed by a PCO device, it is the hydroxyl radical ($OH^{\cdot}$), derived from the oxidation of adsorbed water or adsorbed OH^{-}, that is the dominant strong oxidant. Its net reaction with a VOC can be expressed as:

$$OH^{\cdot} + VOC + O_2 \rightarrow nCO_2 + mH_2O$$

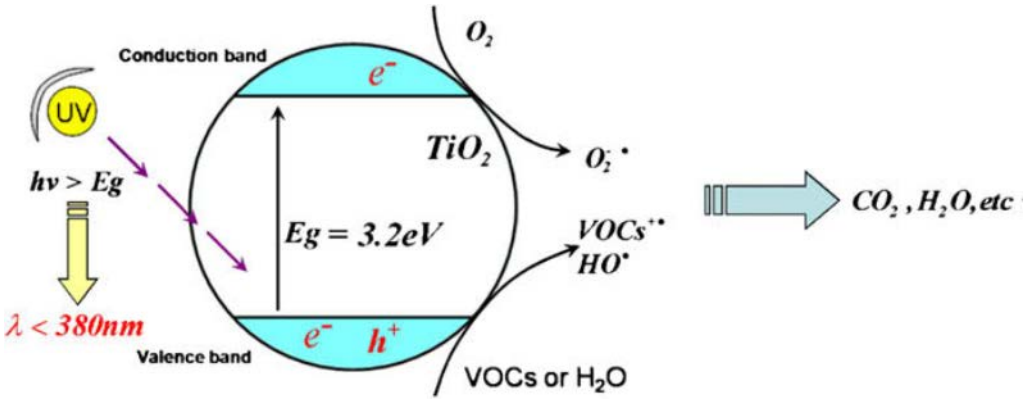

Fig. 2.18. Schematic of TiO_2 UV photocatalytic oxidation process of VOCs.

As a semiconductor material, the band gap (Eg) of ZnO is close to that of TiO_2 [16]. It is reported that the photocatalytic properties of TiO_2 and ZnO are very different in liquid. However, little is well known about the photocatalytic effect of ZnO to degrade volatile organic compounds [53].

Liao et al (2012) [54]compare the photocatalytic properties of TiO_2, ZnO and their composite in the gas phase pollutant environment, nanocomposite with different mole ratios of TiO_2/ZnO were designed to degrade gaseous formaldehyde. The rate constant of TiO2 for formaldehyde degradation was 0.05 min−1 which was two orders of magnitude larger than that of ZnO. and The UV–vis diffuse reflectance spectra of TiO_2 and ZnO samples show the Kubelkka–Mulk absorbance at 365 nm of ZnO is 40% higher than that of TiO2, which means that the absorbability to UV light (365 nm) of ZnO is better than that of TiO_2 as Fig 2.19.

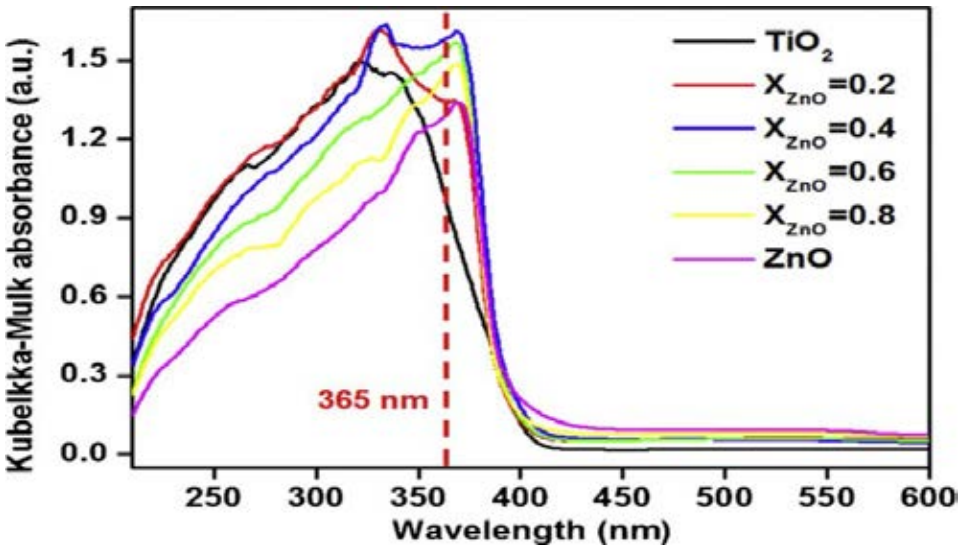

Fig.2.19 UV–vis reflectance spectra of TiO_2/ZnO samples. X_{ZnO} denotes the mole fraction of ZnO in TiO_2/ZnO composite.

He et al. (2003) [30] prepared Polyvinyl alcohol (PVA)–Pt/TiO_2 composite nanofiber by electrospinning method and investigated the photocatalytic degradation of solid-phase PVA. The study revealed that the photocatalytic method could be effective for solid-phase PVA degradation as shown in Fig 2.20. The rate of degradation under UV-C irradiation was about double of that under UV-A irradiation. The weight loss of PVA depended on the wavelength of UV light and the irradiation time.

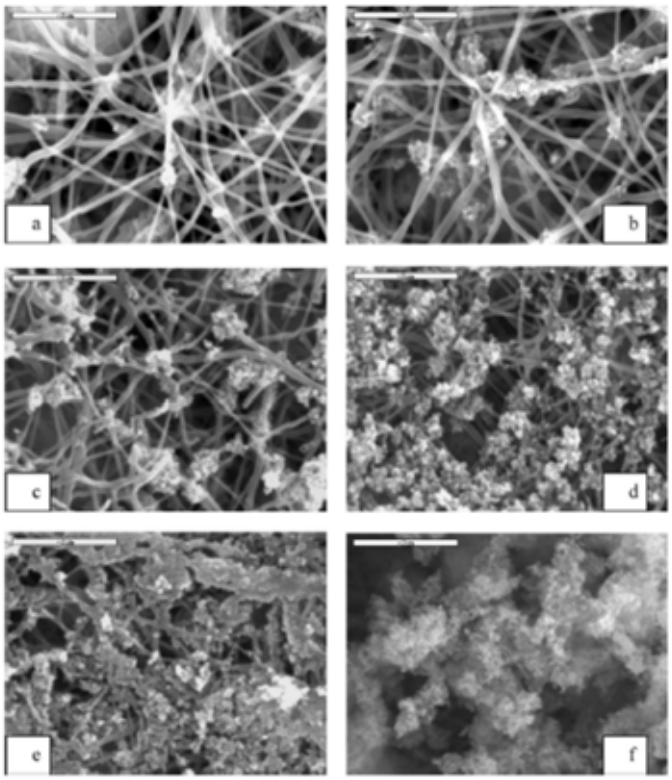

Fig 2.20 SEM images of PVA–Pt/TiO_2 composite fiber mat irradiated under UV-A light at different times: (a) 0 h; (b) 2 h; (c) 4 h; (d) 8 h; (e) 12 h;(f) 16 h.

He et al. [30] suggested the possible reaction for photocatalytic degradation of PVA could be envisioned briefly as follows: The reaction was initiated when the UV light with energy higher than TiO_2 band gap was absorbed by the TiO_2 particles to produce electron (e^-) and hole (h^+) pair in the CB and VB of semiconductor,an d subsequently, trapped by appropriate sites on the TiO_2 surface defects or transferred to species bound to the surface. The CB and VB denote conduction and valence band,respectively.

Following photoexcitation and trapping of charges, surface-adsorbed platinum scavenges away the trapped electrons at the interface, and the electrons react with O_2, leading to the formation of several active oxygen species such as the O_2^- and O_2^{2-} ions. Meanwhile, the adsorbed oxygen tends to react with electrons and hydrogen ions to form water [55]. During the oxidation of organic compound in an aerated system, oxygen was reactive in the cathodic area of the catalyst because of its much higher positive oxidative potential compared with H^+. Especially in the

presence of platinized TiO_2, oxygen was easy to be reduced into hydroxide ions or water [56].

$$TiO_2\,(Pt) + h\nu \rightarrow e^-_{CB} + h^+_{VB}$$

$$e^-_{CB} \rightarrow e^-_{tr}$$

$$h^+_{VB} \rightarrow h^+_{tr}$$

$$O_{2(ads)} + 2H^+ + e^-_{tr} \rightarrow 2OH^-$$

$$OH^- + H^+ \rightarrow H_2O$$

$$O_{2(ads)} + e^-_{tr} \rightarrow O_{2(ads)}$$

$$-(CH_2\,CH(OH)\,CH_2CH(OH)\,CH_2)- + h^+_{tr} \rightarrow -(CH_2\,\dot{C}\,(OH)\,CH_2CH(OH)\,CH_2)- + H^+$$

$$-(CH_2\,\dot{C}\,(OH)\,CH_2CH(OH)\,CH_2)- + h^+_{tr} \rightarrow -(CH_2\,COCH_2CH(OH)\,CH_2)- + H^+$$

$$-(CH_2\,COCH_2CH(OH)\,CH_2)- + H_2O + h^+_{tr} \rightarrow -(CH_2\,COOH + \dot{C}H_2\,CH\,(OH)\,CH_2- + H^+$$

$$\rightarrow\rightarrow \text{Successive cleavage} \rightarrow CO_2 + H_2O$$

Simultaneously, the trapped holes oxidize the PVA matrix resulting in the formation of carbonyl bonds and the scission of carbon–carbon bonds occurs once the oxygen is introduced by reaction with water. The successive reactions result in the chain cleavage and the formation of mineralized product. There were various possible pathways were assumed for photocatalytic degradation of organic compounds [57, 58]. One is direct oxidation: the organic compound adsorbed onto the anodic surface of the photocatalyst may be oxidized directly by holes and mineralized finally to CO_2. Another was indirect oxidation: the organic compound adsorbed onto the catalytic surface may be oxidized indirectly by attack of hydroxyl radicals ($^{\cdot}OH$) which were formed by photoproduced holes.

CHAPTER III

EXPERIMENT

3.1 Chemicals

Chemicals which were used in this study were described as follows:-

1. Polyvinylpyrolidone (PVP), Mw ~ 1,300,000, (produced by Sigma-Aldrich Chemical Company) was used on the basis of as received.

2. Zinc oxide (ZnO)(produced by Ajax Finechem Pty Ltd) was used on the basis of as received.

3. Sodium hexametaphosphate (produced by Ajax Finechem Pty Ltd) was used on the basis of as received.

4. Ethanol absolute AnalaR NORMAPUR (99.8%) (produced by VWR International Company) was used on the basis of as received.

3.2 Experimental Procedures

3.2.1 Fabrication of nanofibers

3.2.1.1 PVP nanofiber Fabrication

PVP was dissolved in ethanol to prepare 8, 10 and 12 wt.% solution respectively. Each solution was stirred for 60 minutes. An electrospinning equipment was used to produce nanofibers at the applied voltages of 13, 17 and 21 kV and a distance between the collector and the tip of the syringe needle was 20 cm. The obtained fibers were further to examined for their properties. The conductivity and viscosity of PVP solution was also determined.

3.2.1.2 PVP/ZnO nanofiber Fabrication

The preparation of PVP/ZnO nanofibers was done as the following steps and the contents of materials in the mixture and conditions of voltage power supply were illustrated in Table 3.1.

Firstly the ZnO powder in ethanol mixture was prepared by dispersing the designated amount of ZnO powder in 10 ml ethanol. When the tests required the addition of dispersant, the ZnO powder mixture was added with 0.3% sodium hexametaphosphate solution which was prepared by dissolving sodium hexameta phosphate in a few drop of water before mixing. Each suspension of ZnO powder in ethanol mixture with dispersant or without one was ultrasonicated for 60 minutes to make sure its well dispersion and to prevent of ZnO agglomeration.

The second task was preparation of PVP in ethanol solution. The designated amount of PVP material as described in Table 3.1 was dissolved in 15 ml ethanol to obtain 8, 10 and 12 percent weight of PVP in solutions respectively. The mixture of PVP/ethanol solution was then stirred for 60 minutes to produce a well clear solution for further mixing.

The third task was preparation of PVP/ZnO solution for electrospinning fibers. The well disperser mixture of ZnO powder was mixed with PVP/ethanol solution to result weight ratios of PVP to ZnO varying from 5:1, 5:3, 5:5, 5:10, 5:20, 5:30 to 5:50 as described in Table3.1. This PVP/ZnO mixture was then ultrasonicated for 60 minutes and followed by continuously stirring for 24 hours. The obtained PVP/ZnO mixture was ready for nanofiber production. In practice, the PVP/ZnO nanofiber was fabricated using the eletrospinning equipment as showed in Fig. 3.1. The electrospinning equipment consisted of a collector, a syringe with needle and high voltage power supply. The collector was covered with an aluminum foil to serve as a counter electrode for collecting the electrospun which could be observed as dense web of fibers depositing on the surface of aluminum foil. In operation, the power supply would generate the different electric potential voltage between a needle tip and a collector and a range of 13-21 kV.

Table3.1 The compositions and conditions for the preparation of PVP/ZnO nanofibers

Quantity of PVP in ethanol (wt%)	**Ratios of PVP to ZnO (by weight)**	**Applied voltage (kV)**
8	5:10	17
10	5:01	13, 17, or 21
	5:03	
	5:05	
	5:10	
	5:20	
	5:30	
	5:50	
12	5:10	17

For nanofiber fabrication, the PVP/ZnO mixture was filled into the syringe and installed in its position in the electrospinning equipment. The distance between the needle tip and the equipment base was 24 cm in height and the distance between the needle tip and the collector covered with aluminum foil was 20 cm. Then high voltage power supply was switch on to generate the electric different potential voltage by gradually increasing from zero to the required voltage of 13, 17 or 21 kV. After the system was fully supplied by the required electric voltage, the PVP/ZnO mixture moved from needle tip to collector and it was changed from droplet to fibers. The phenomena of fiber generation was ready described in chapter 2. In this study, particle size distribution of ZnO in ZnO/PVP suspension was examined by laser light scattering (Malvern mastersizer). The Brunauer-Emmett-Teller (BET) was employed to determine the surface area of ZnO particles. Electron microscopy was also employed to characterize morphology of ZnO particles and the composite ZnO/PVP nanofibers.

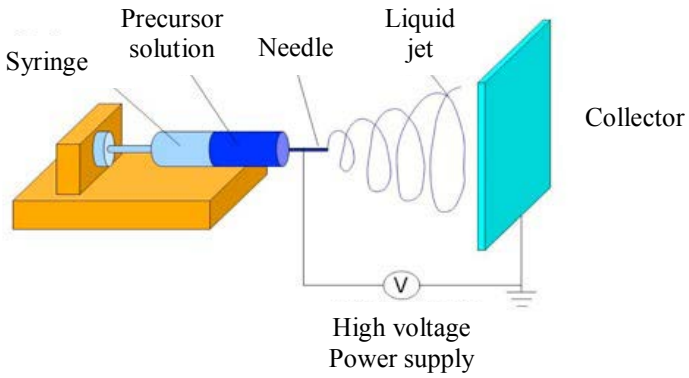

Fig.3.1 Schematic diagram of Electro spinning equipment.

3.2.1.3 Summary of Electrospinning Conditions

Height (H)	=	24 cm.
Distance (D)	=	20 cm.
Voltage	=	13, 17, 21 kV
Weight percent of PVP	=	8, 10, 12 wt%
PVP to ZnO ratios	=	5:1, 5:3, 5:5, 5:10, 5:20, 5:30 and 5:50

3.2.2 Photocatalytic degradation of Solid phase PVP

The photocatalylic degradation reactions of PVP/ZnO nanofibers were carried out under atmospheric condition in a reactor as showed in Fig.3.2. The reactor consisted of the irradiation source generation from a UV-A lamp of Phillips TLD 15W/05. The circular trays provided the irradiation distance of 10 cm between lamp surface and sample exposed surface of which the test sample was attached on the circular tray. For testing, all fiber samples were prepared as a rectangular mat with area of 24 cm^2. This rectangular mat would contain about 20-30 mg of the fiber weight. The exposure periods of UV light for the PVP/ZnO nanofibers were 0, 1, 3, 6, 12, 24 and 48 hours. After the irradiation of the PVP/ZnO nanofibers was completed, the studied samples were further characterized. For examples, each

sample was employed by using thermogravimetric and differential thermal analyzer (TG/DTA) to examine weight ratios of PVP and ZnO on nanofibers before and after irradiation. The weight loss of PVP by photocatalytic degradation was calculated as the function of irradiation time. The morphology was investigated by Electron microscopy.

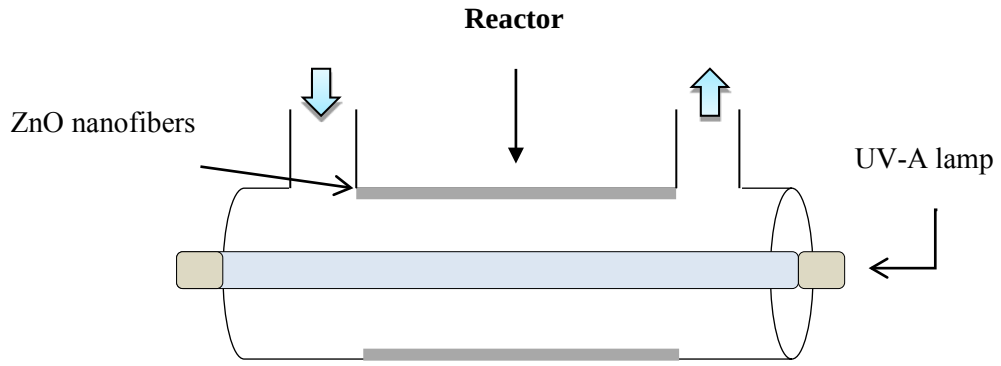

Fig. 3.2 Schematic diagram of UV degradation reactor

3.2.3 Characterizations

The PVP/ZnO mixture, the fabricated ZnO/PVP nanofibers and the UV-A irradiated ZnO/PVP nanofibers were characterized by various analytical techniques.

3.2.3.1 Viscomiter

The viscosities of mixtures were measure by using Rheocalc V3.3 Build 49-1,Brookfield Rheometer model RVDV-11+PRO shown in Fig 3.3 at Center of Excellence in Particle and Technology Engineering laboratory, Chulalongkorn University.

Fig.3.3 Viscometer

3.2.3.2 Mastersizer

Particle size distribution of ZnO in ZnO/PVP suspension was examined by using the laser light scattering (Malvern mastersizer 2000) asc shown in Fig 3.4 at Center of Excellence in Particle and Technology Engineering laboratory, Chulalongkorn University.

Fig.3.4 Mastersizer

3.2.3.3 Scanning Electron Microscopy (SEM)

The morphology of ZnO particles, PVP nanofibers and composite ZnO/PVP nanofibers were determined by using JEOL scanning electron microscopy model JSM-6400 as shown in Fig 3.5 at The Scientific and Technological Research Equipment Center (STREC), Chulalongkorn University.

Fig.3.5 Scanning Electron Microscope

3.2.3.4 Transmission electron microscope (TEM)

The structures of PVP/ZnO fibers were investigated by using JEOL transmission electron microscopy model TEM, JEOL JEM-2010 as shown in Fig.3.6 at the Scientific and Technological Research Equipment Center (STREC), Chulalongkorn University.

Fig.3.6 Transmission Electron Microscopy

3.2.3.5 Thermogravimetric analysis (TGA)

The decomposition temperature and thermal behavior of the fiber products, weight ratios of PVP and ZnO on nanofibers and the weight loss of PVP photocatalytic degradation were studied by using Thermogravimetric analysis on a Mettler-Toledo TGA/DSC1 STARe System as shown in Fig.3.7 at Center of Excellence in Particle and Technology Engineering laboratory, Chulalongkorn University. The samples were heated from 25^{o}C to 1000^{o}C under the oxygen flow rate of 40 ml/hr and the ramp rate of 10 °C/min.

Fig.3.7 Thermogravimetric analysis (TGA)

3.2.3.6 Fourier-transform infrared spectroscopy (FT-IR)

A Fourier transform infrared spectrometer (Nicolet 6700) at Center of Excellence in Particle and Technology Engineering laboratory, Chulalongkorn University were used to investigate the functional group in the products. The samples were mixed with KBr in a ratio of sample to Kbr 1:100 before measurement. The spectra were recorded at wavenumber between 400 and 4000 cm^{-1} with resolution of $2cm^{-1}$

Fig.3.8 Fourier-transform infrared spectroscopy (FT-IR)

3.2.3.7 Conductivity Meter

PVP/ZnO mixture was indirectly analyzed by using the electroconductivity meter (FR30, Mettler Toledo) at Center of Excellence in Particle and Technology Engineering laboratory, Chulalongkorn University to measure the conductivity of mixture.

Fig.3.9 Conductivity Meter

3.2.3.8 The Brunauer-Emmett-Teller (BET)

The Brunauer-Emmett-Teller (Belsorp II) as shown in Fig.3.10 at Center of Excellence in Particle and Technology Engineering laboratory, Chulalongkorn University was employed to determine the surface area of ZnO particles.

Fig.3.10 Brunauer-Emmett-Teller (BET)

CHAPTER IV

RESULTS AND DISCUSSION

This chapter is devoted for describing all results of analysis and characterization of synthesized products. The fabricated PVP and PVP/ZnO nanofibers were characterized by various analytical techniques. Effects of weight percent of PVP in ethanol, PVP/ZnO weight ratio and electrical potential employed for electrospinning process on the uniformity of ZnO embedding in PVP/ZnO nanofibers was discussed. In the final part of this chapter, the fabricated PVP/ZnO nanofibers which were situated in a photo reactor, were examined to reveal its stability for VOC removal.

4.1 Fabrication PVP nanofibers

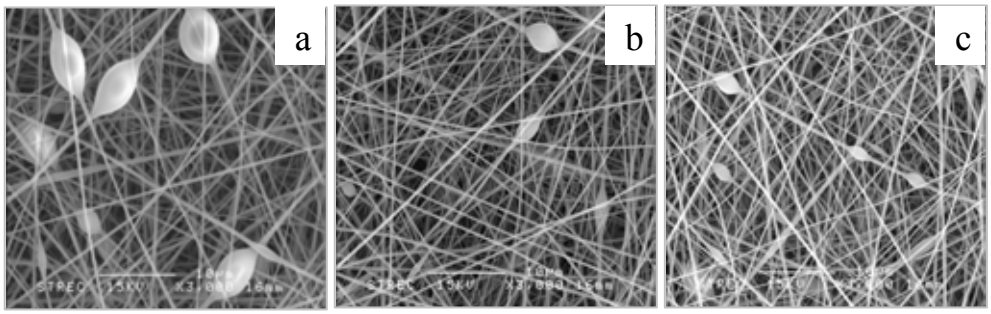

Fig.4.1 SEM micrographs of PVP nanofibers using 8wt% of PVP to Ethanal solution and varying applied voltage (a)13kV, (b)17kV, (c) 21kV

Morphology of PVP fibers spun by 3 different voltages is compared by typical SEM images shown in Fig.4.1. Such PVP fibers were fabricated from 8 weight percent of PVP in ethanol with the supplied voltage of 13kV, 17kV and 21kV. When the voltage for electrospinning was increased, PVP fibers with smaller diameter were obtained. However, some bead was also detected. Smaller beads were formed when the electrical voltage was increased. This result would be ascribed that capillary instability plays a role in fiber formation. A cylindrical jet of PVP solution would occasionally collapse into separated droplets which would be solidified, when the electrical voltage supplied to the jet was reduced [59]. Fong et al. [60] suggested that if the solution viscoelasticity for electrospinning was

increased, the jet against the formation of beads could be stabilized, resulting in formation of small beads

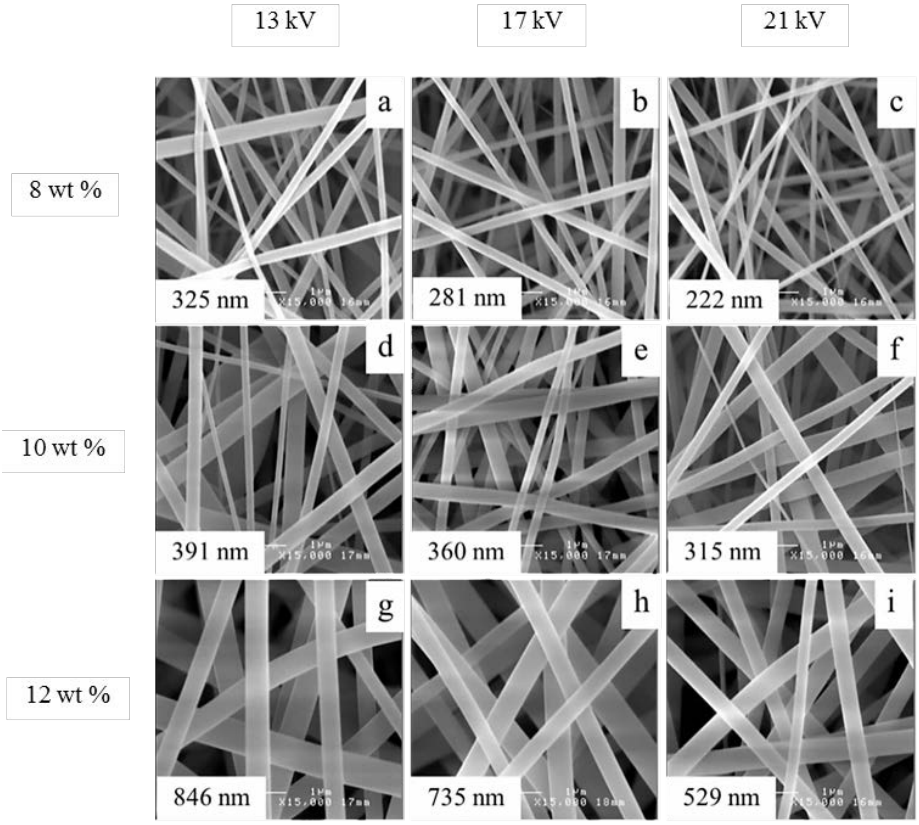

Fig.4.2 SEM micrographs of PVP composite using (a)(b)(c) 8wt%, (d)(e)(f) 10wt% , (g)(h)(i) 12%wt of PVP and vary Voltage (a)(d)(g) 13kV, (b)(e)(h) 17kV, (c)(f)(i) 21kV

When the concentration of PVP was increased, the PVP fibers with larger diameter were obtained as showed in Fig 4.2. The increase in weight percent of PVP to ethanol from 8,10 to 12 weight percent resulted in the PVP fibers with average diameter of 325nm, 391,nm and 846nm, respectively when the electrospinning voltage was 13 kV. Similarly, when the supplied voltage was 17kV, increase in the weight percent of PVP to ethanol could provide the PVP fiber with average diameters of 281, 360 and 735 nm, respectively. With the supplied voltage of 21kV, PVP fiber with average diameters of 222nm, 315nm, 529nm could be produced from the 8, 10 and 12 weight percent PVP in ethanol solution respectively.

Fig 4.3 showed the viscosity of PVP/ethanol solution was elevated with the increased concentration of PVP. The viscosity of the PVP/Ethanol solution was gradually increased when the PVP in ethanol solution was increased from 8 weight percent to 10 weight percent but the 12 weight percent PVP in ethanol solution resulted in a sharp increase in the viscosity up to 600 centipoise.The increase in the viscosity of the PVP/ethanol solutions could lead to non-uniform ejection of the jet [13].

The average diameters of the PVP nanofiber became smaller when the applied voltage was increased as the electrostatic field strength became increased. This increased electrical voltage could affect an increase in both the electrostatic force, which would be responsible for the electron transport in the charged jet injected to the aluminium foil collector, leading to an increase in the mass throughput of the PVP and the Coulombic repulsion force. Such Coulombic repulsion force would be responsible for the stretching of the ejected jet , leading to a decrease in the fiber diameters[13].

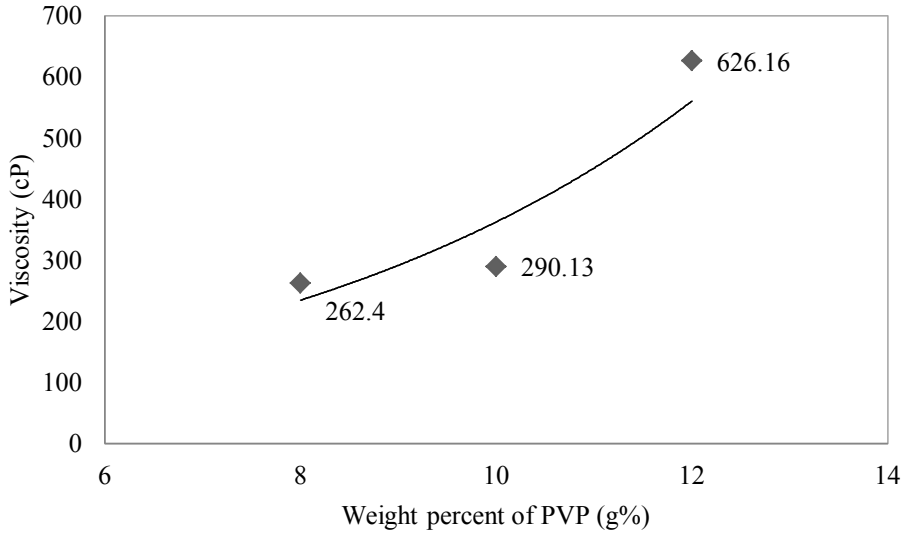

Fig.4.3 dependence of PVP/ethanol with viscosity on PVP weight percent

4.2 Fabrication PVP/ZnO nanofibers

4.2.1 Dispersion of ZnO in ethanol

Fig.4.4 showed typical micrographs of ZnO powders under different conditions. For comparison, Fig. 4.4 (a) shows that commercial ZnO particles exhibited a rigorous agglomeration, resulting in an average particle size of 402 nm. Fig. 4.4(b) illustrated that ZnO samples which were subjected to the mechanical stirring had bigger agglomerates with an average size of 473 nm. Such mechanical stirring would provide a higher possibility of ZnO particle collision, which collision would lead to a higher possibility of agglomeration. Meanwhile, as could be observed in Fig.4.4(c), ZnO powders suspension in ethanol which was subjected to ultrasonication had a smaller average size of 285 nm. When 0.3wt% sodium hexametaphosphate dispersant was added into the suspension of ZnO in ethanol, dispersion of ZnO particles could be improved as observed in Fig. 4.4(d). Such ZnO samples added with sodium hexametaphosphate dispersant and subject to ultrasonication exhibited smaller particle size than those of previous samples without dispersant The smaller mean particle size of 278 nm would be attributed to the cavitations incorporated with the increase in surface change of ZnO particles due to the presence of dispersant.

The similar results were observed by Chung et al. when ultrasonication of ZnO nanoparticles in ethanol would undergo the effective dispersion due to cavitation mechanism. In general, ZnO particles would form agglomerate due to the effect of the van der waals force and liquid surface tension. When the ZnO particles are ultrasonicated, the ultrasonic wave would generate additional stress onto liquid matrix, resulting in formation of uniform and tiny cavitations moving with supersonic speed. Such cavitations could cause extremely high pressure stress which were beneficial to separate each suspending particles apart from each other [10].

The results based on application of dispersant would suggest that better dispersion of ZnO in ethanol could be improved by the synergetic effect of ultrasonic

cavitation and sodium hexametaphosphate dispersant. Dispersant could produce surface charges, resulting in strong repulsive force acting on each individual ZnO particle. In comparison of the dispersion method, the surface area of 2.554 m^2/g which was obtained from ZnO particles added the dispersant was larger amount than that of the ZnO particles without dispersant addition. The surface area of ZnO particles without adding dispersant was 2.086 $m^{2/}g$.

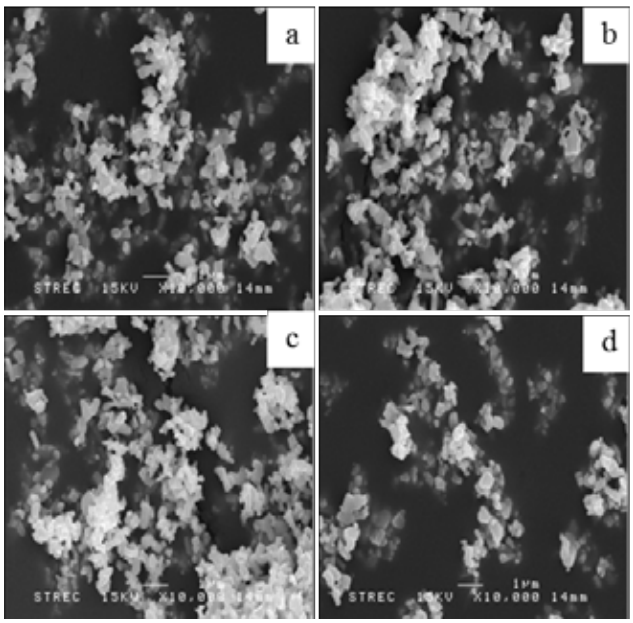

Fig.4.4 SEM micrographs of ZnO powder (a) as-received sample (b) sample subject to mechanical stirring (c) sample subject to ultrasonication and (d) sample + 0.3 wt% dispersant subject to ultrasonication

As shown in Fig.4.5, these is a tendency that ultrasonication with and without dispersant would result in a lower degree of agglomeration of ZnO particles. This result would suggest that application of dispersant and ultrasonication would be essential for uniform dispersion of ZnO in liquid. Therefore, in order to prepare a uniform dispersion of ZnO in PVP/ethanol solution, both Sodium hexametaphosphate and ultrasonication would be applied.

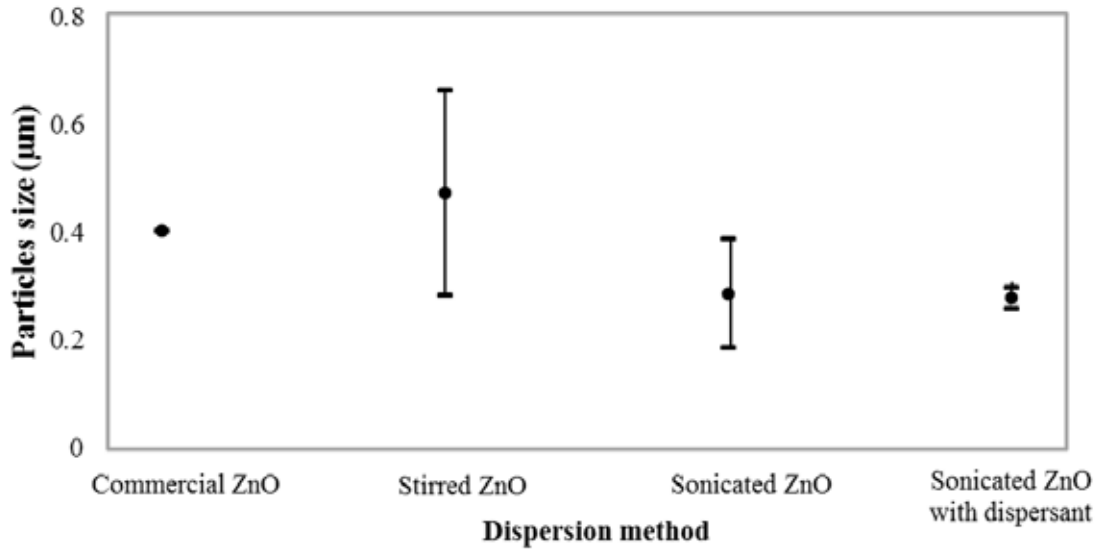

Fig.4.5 Average particle size of ZnO powder (1) as-received sample (2) sample subject to mechanical stirring (3) sample subject to ultrasonication and (4) sample + 0.3 wt% dispersant subject to ultrasonication

An increase in surface polarity was obtained from ZnO particles adding with sodium hexametaphosphate dispersant, when FT-IR spectroscopic analyses of all samples were taken into account. As shown in Fig.4.6, samples of as received ZnO which were treated by mechanically stirred ZnO and ultrasonicated exhibited insignificantly different IR spectra. In the IR spectra of ZnO paticles as showed Fig 4.6 (a), the 3425 and 533 cm^{-1} band were derived from O-H stretching and Zn-O respectively. The P-O stretching bands at 1052cm^{-1} of Sodium hexametaphodphate was also observed in ZnO particles with dispersant.

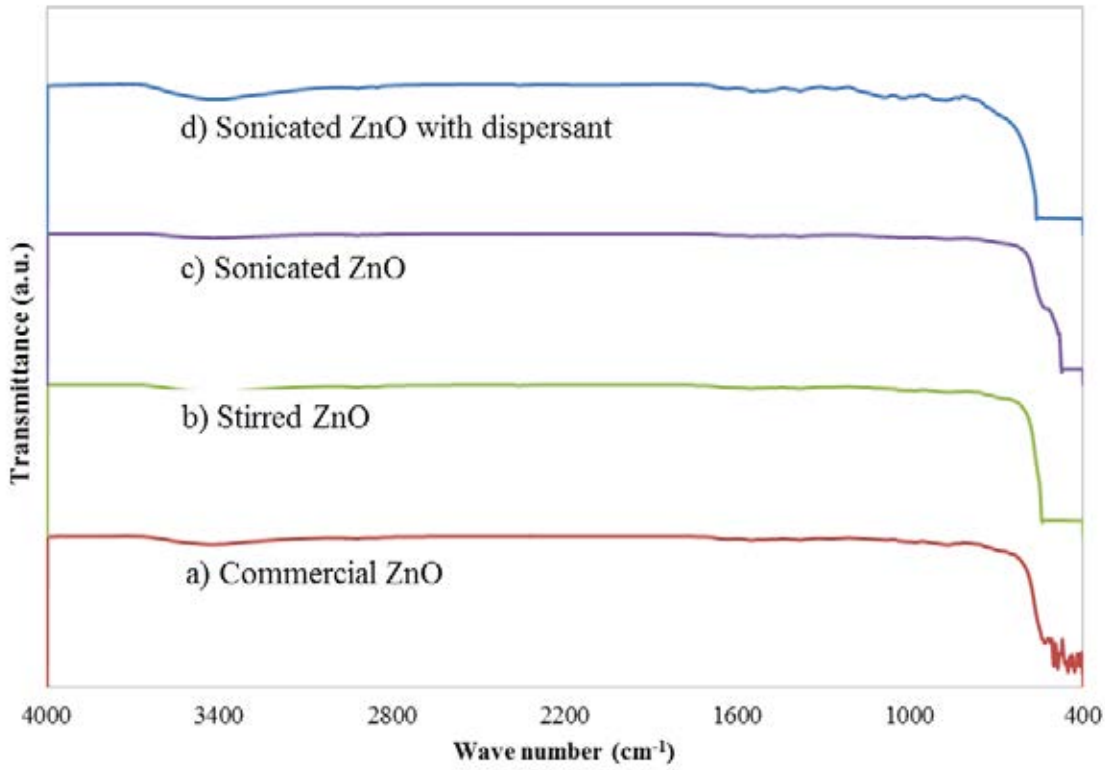

Fig.4.6 Comparison of FT-IR spectra of ZnO powder (a) as-received sample (b) sample subject to mechanical stirring (c) sample subject to ultrasonication and (d) sample + 0.3 wt% dispersant subject to ultrasonication.

The ZnO sample which was added with sodium hexametaphosphate and ultrasonicated exhibited some distinctive peaks. Such analytical results would suggest that some radicals, which were generated from the dissociated sodium hexametaphosphate, would be induced by ultrasonication and then deposited onto the surface of ZnO particles [61]. The better dispersion of ZnO in ethanol could be obtained. Therefore, lower agglomeration of ZnO particles would be anticipated to provide suspension of uniformly dispersed ZnO. The ZnO dispersion could be beneficial to the better mixing with PVP solution.

4.2.2 Fabrication of PVP/ZnO nanofibers

4.2.2.1 Effect of dispersing method

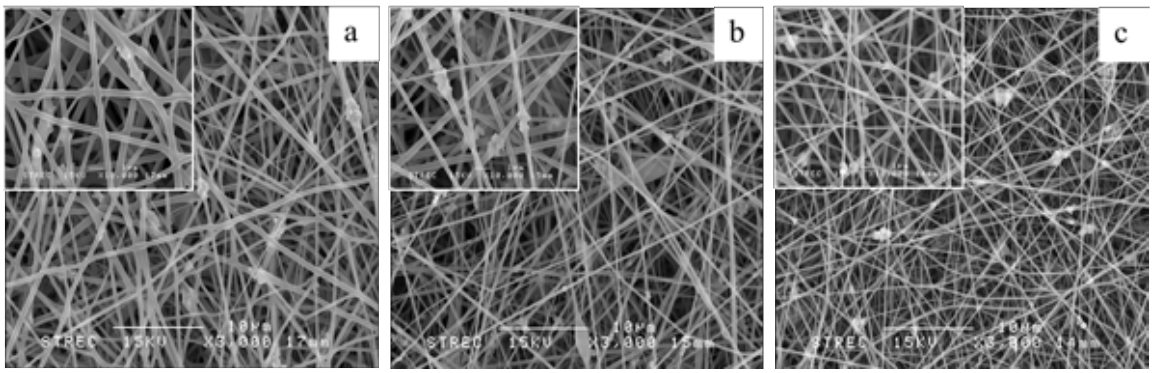

Fig.4.7 SEM micrographs of PVP/ZnO nanofiber prepared from different ZnO suspension (a) sample dispersed by mechanical stirring, (b) sample dispersed by ultrasonication, and (c) sample dispersed by ultrasonication with dispersant

In general, the dispersing method could affect the degree of agglomeration of ZnO particles which are suspended in a liquid. Therefore, in this research ZnO powders were dispersed in PVP under the condition of ultrasonicate with dispersant in prior to the electrospinning of PVP/ZnO nanofibers. Verification of ZnO dispersion will be described further.

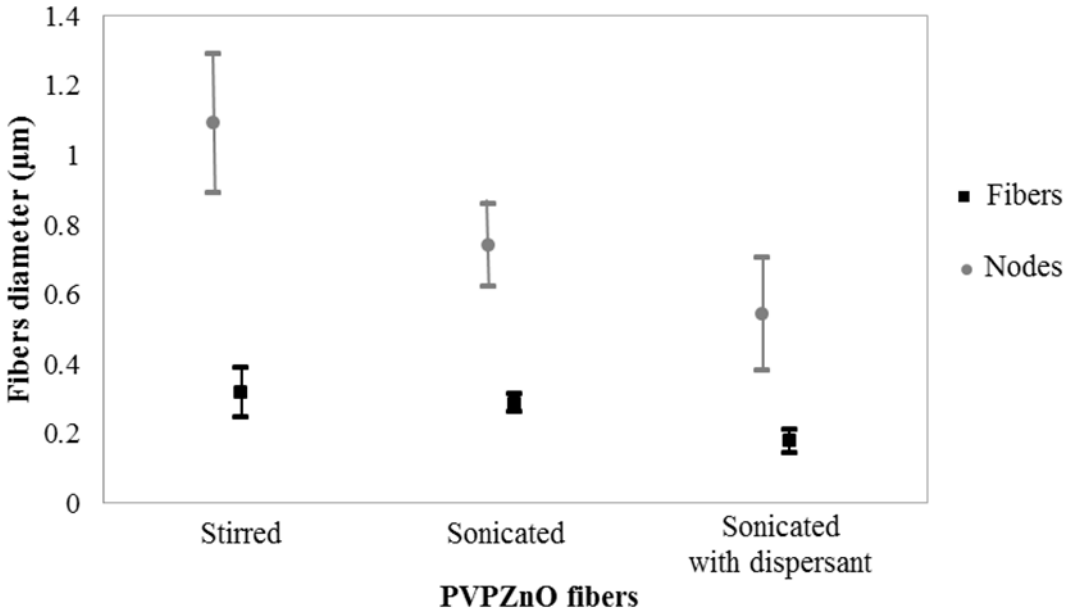

Fig.4.8 Average particle size of PVP/ZnO fibers prepared from different ZnO suspension sample dispersed by mechanical stirring,sample dispersed by ultrasonication, and sample dispersed by ultrasonication with dispersant.

Fig.4.7 showed typical SEM micrographs of PVP/ZnO nanofibers which were prepared from suspension of ZnO dispersed by 3 different methods. Fig. 4.7(a) revealed the PVP/ZnO nanofibers prepared from ZnO suspension, which was subjected to mechanical stirring. A relatively non-uniform size with agglomeration of ZnO particles was obtained. Based on the image processing, the average fibers and nodes diameter sizes were 0.316 and 1.09 µm, respectively. For the ZnO suspension subject to ultrasonication, fibers with uniform diameter were obtained as shown in Fig. 4.7 (b). However agglomeration on ZnO particles could be observed. Also the image processing analysis reveals that, the average fibers and nodes diameter size were 0.287 and 0.741 µm, respectively. Meanwhile, PVP/ZnO nanofibers which were prepared from ZnO suspension with the presence of sodium hexametaphosphate and subjected to ultrasonication is showed Fig. 4.7 (c) It could be observed that the PVP/ZnO nanofibers exhibited uniformly and narrow size distribution. The average size of fibers and nodes diameter base on the image processing were 0.176 and 0.543 µm, respectively. These results would be attributed to the presence of sodium hexametaphosphate, resulting in a significant increase in

the conductivity of PVP/ZnO suspension from 2.36 to 10.19 us/cm. Such higher electroconductivity could enhance capability of charges and effectively spun by the electrospinning method. In addition, ZnO particles were well dispersed within the PVP matrix and small amount of ZnO agglomeration could be obtained. Thus ZnO particles could be uniformly embeded within the smaller diameter fibers.

Park et al.[61] suggested that sodium hexametaphosphate resulted high zeta potential of about −88.2 mV. The ZnO nanopowder surface was covered by Na^+ ions. Then the positively charged ZnO nanopowders repulse each other.

In order to confirm the uniformity of ZnO dispersion within the PVP/ZnO nanofibers, TEM analyses were also conducted. As could be observed in Fig. 4.9(a) and 4.9 (b), ZnO particles within the PVP/ZnO nanofibers prepared from the ZnO suspension which was subject to ultrasonication only, exhibited higher degree of forming agglomeration when compared with that of the PVP/ZnO nanofibers which were prepared from the ZnO suspension subject to ultrasonication with the presence of sodium hexametaphosphate dispersant.

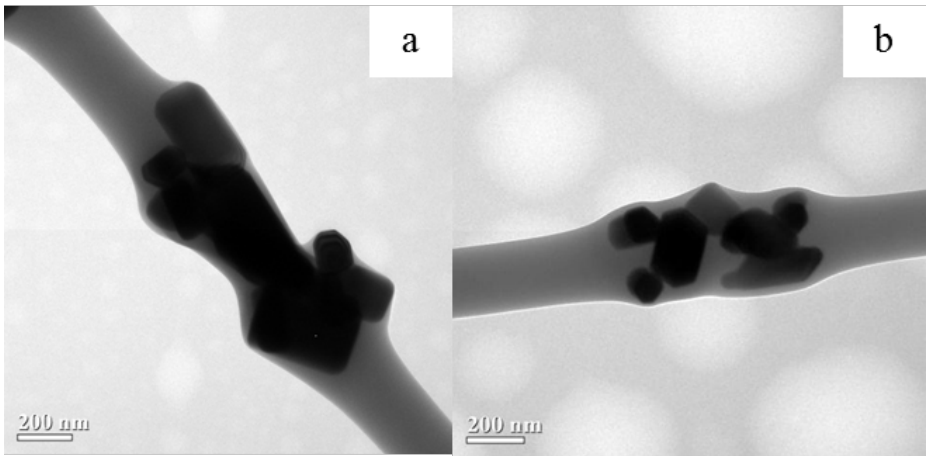

Fig.4.9 TEM micrographs of PVP/ZnO nanofibers were prepared from ZnO suspensions (a) subjected to ultrasonication only and (b)subjected to ultrasonication with the presence of sodium hexametaphosphate.

4.2.2.2 Effect of the weight percent of PVP to ZnO

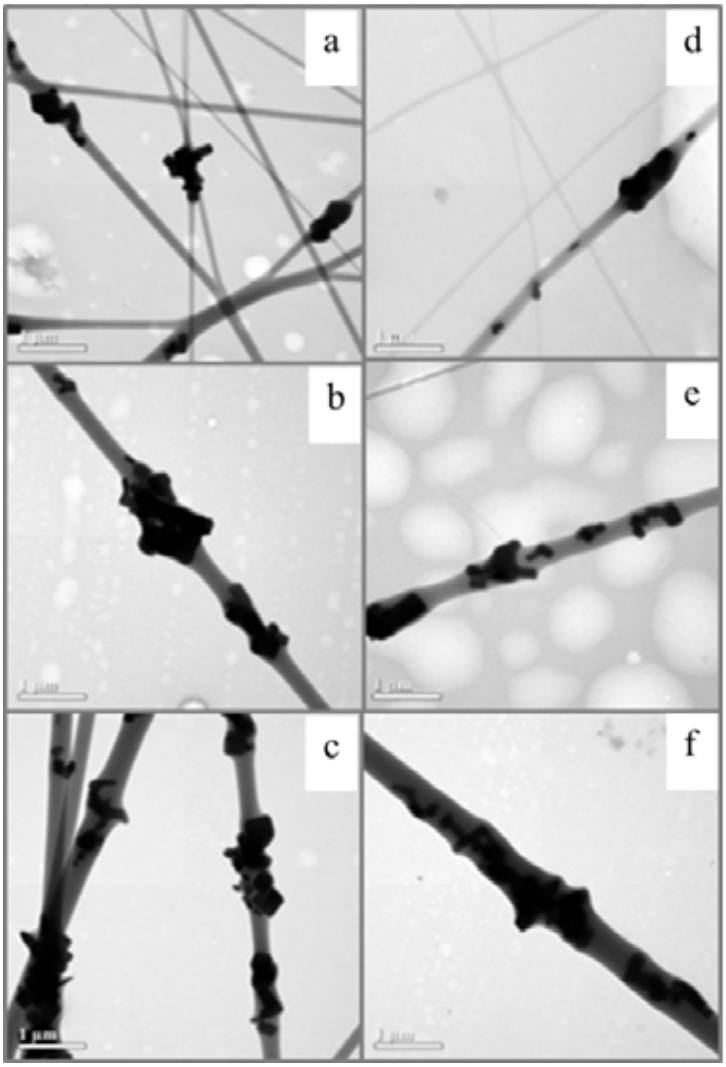

Fig.4.10 TEM micrographs of PVP/ZnO fibers which the weight ratio of PVP to ZnO equal to 5:10 using applied electrical voltage 17 kV and and varying the weight percent of PVP in ethanol (a)8 wt%, (b) 10 wt% and (c) 12wt%, (a, b, c) without dispersant, (d, e, f) with dispersant.

Fig.4.10 exhibited the effect of the weight percent of PVP to ethanol. When the concentration of PVP was increased, fibers diameter was increased. The increase in the viscosity of the PVP solutions could lead to non-uniform ejection of the jet [13]. In comparison of the distribution of ZnO particles imbedded in PVP polymer matrix, the big size diameter fiber could be obtained with ZnO particles distributing in the hold fiber as shown in Fig 4.10c, 4.10f and Fig 4.11c, 4.11f. For small size

diameter fiber, node distribution and non-uniformity were obtained from PVP/ZnO fibers at 8 weight percent of PVP to ethanol (4.10a, 4.10d and 4.11a, 4.11b). For this weight percent, beads were formed on fibers. These results could be attributed to the capillary instability that caused a cylindrical jet of liquid to collapse into separated droplets occurred when the excess electrical charge which was carried by the jet was reduced. This structure droplets solidified to form beaded nanofibers [17]. From the results, presentation of ZnO particles were not only imbedded in PVP polymer ducts but also in beads as shown in Fig 4.10a and 4.11a.

The comparison of the distribution of ZnO particle imbedded in PVP polymer matrix using the different dispersion method was shown in fig 4.10, the resulting ZnO particles imbedded in the fibers with dispersant had better uniformity than the fibers produced from the solution without dispersant. This result could be attributed to that the Sodium hexametaphosphate dispersant would provide surface charge, resulting in strong repulsive force acting on each individual ZnO particle.

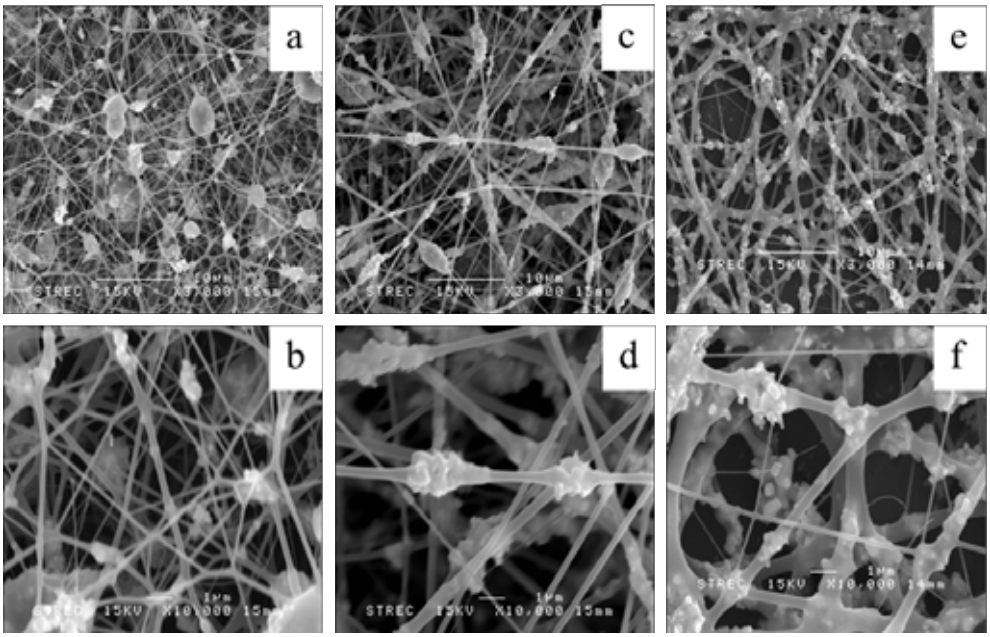

Fig. 4.11 SEM micrographs of PVP/ZnO nanofibers which the weight ratio of PVP to ZnO equal to 5:10 using 17 kV applied electrical voltage and varying weight percent of PVP in ethanol (a, b) 8wt% , (c, d) 10wt% and (e, f) 12wt% in resolution x3000 and x10000.

Table 4.1 showed the comparison of theorical and actual weight ratios of PVP to ZnO which were varied by the weight percent of PVP to ethanol. The weight ratios of PVP to ZnO fibers were examined via weight loss calculation by using Thermogravimetric analysis. In comparison with all weight percent of PVP to ZnO, the maximum actual weight ratios of PVP to ZnO fibers of 5:9.84 was obtained from the weight percent of PVP to ethanol of 10 weight percent fibers. The minimum actual weight ratios of PVP to ZnO fibers of 5: 8.00 was obtained from the 12 weight percent of PVP to ethanol.

The morphology of fiber fabrication with varying the weight percent of PVP to Ethanol was summarized in table 4.1

Table 4.1 Summary results of the fabrication of PVP/ZnO fibers

Condition		**Actual weight ratios (without dispersant)**	**The average diameter size (Fig) 4.10**		**Fibers morphology**
Theorical weight ratios	**Weight percent**		**Fibers**	**Nodes**	
5:10	8wt%	5:8.78	153 nm	517 nm	Small size diameter with large amount of beads. The average beads size was 2.1 micrometer , ZnO particles mainly distributing in beads and nodes
5:10	10wt%	5:9.84	274 nm	777 nm	Medium size diameter, ZnO fairly distributing in both nodes and fibers
5:10	12wt%	5:8.00	357 nm	989 nm	Large size diameter ZnO particles mainly distributing in fibers rather than nodes.

4.2.2.3 Effect of electrical force

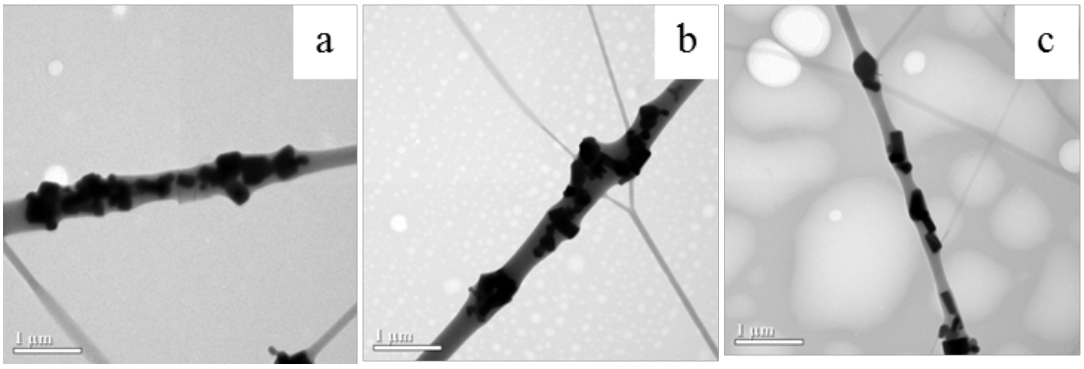

Fig. 4.12 TEM micrographs of PVP/ZnO nanofibers which the weight ratio of PVP to ZnO equal to 5:10 using 10 weight percent of PVP in ethanol and varying applied electrical voltage (a)13kV, (b) 17 and (c) 21kV

TEM images in Fig.4.12 show the morphology of PVP/ZnO fibers without dispersant. The diameter of the nanofiber was smaller when the applied voltage was increased. This result is ascribed to the increasing the Coulombic repulsion force which was responsible for the stretching of an ejected jet segment [13].

Comparison of the dispersion of ZnO particles imbedding in PVP polymer matrix would suggest that the fiber with a larger diameter could accommodate ZnO particles with better dispersion. For the fibers with smaller diameter, formation of polymer droplets at junction of entangling fibers which is called as “node” could be observed as shown in Fig 4.12 and Fig 4.13.

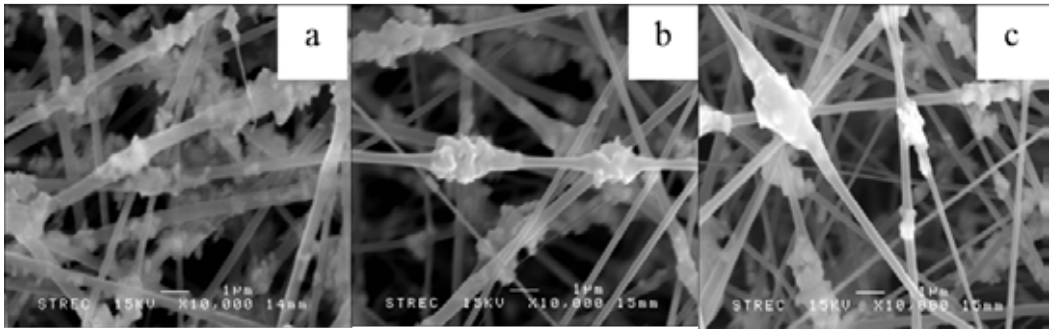

Fig. 4.13 SEM micrographs of PVP/ZnO nanofibers which the weight ratio of PVP to ZnO equal to 5:10 using 10 weight percent of PVP in ethanol and varying applied electrical voltage (a)13kV, (b) 17 and (c) 21kV.

Table 4.2 showed the comparison of theorical and actual weight ratios of PVP to ZnO when the applied voltages were varied. The weight ratios of PVP to ZnO fibers equal to 5:10 were examined via weight loss calculation by using Thermogravimetric analysis. In comparison with all applied voltage, the maximum actual weight ratios of PVP to ZnO fibers of 5:10.32 was obtained from the applied voltage of 13kV fibers due to their larger diameter of fibers. ZnO particles could be distributed in the hold fiber. While the minimum actual weight ratios of PVP to ZnO fibers of 5:5.48 was obtained from the applied voltage of 21kV fibers and their smaller diameter of fibers was produced, ZnO particles were presented in node distribution with non-uniformity as shown in Fig 4.10. But at this moment, the resulted cannot be explained.

The morphology of fiber fabrication with varying the applied voltage supply was summarized in table 4.2

Table 4.2 Summary results of the fabrication of PVPZnO fibers

Condition		**Actual weight ratios (without dispersant)**	**The average diameter size (Fig) 4.10**		**Fibers morphology**
Theorical weight ratios	**Voltage**		**Fibers**	**Nodes**	
5:10	13kV	5:10.32	334 nm	751 nm	Large size diameter, ZnO particles mainly distributing in fibers rather than nodes
5:10	17kV	5:9.84	274 nm	777 nm	Medium size diameter, ZnO fairly distributing in both nodes and fiber
5:10	21kV	5:5.48	248 nm	765 nm	Small size diameter ZnO particles mainly distributing in nodes and a few in fibers.

4.2.2.4 Effect of the weight ratio of PVP and ZnO

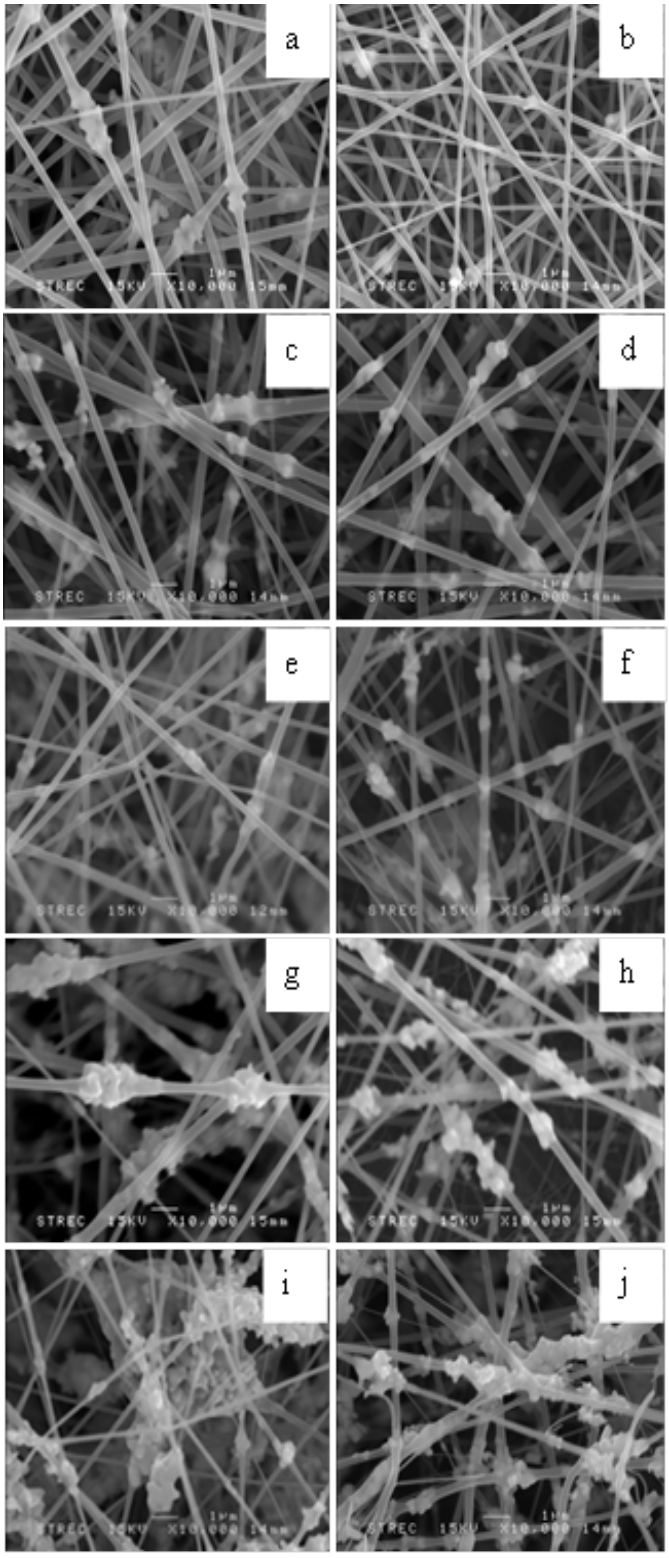

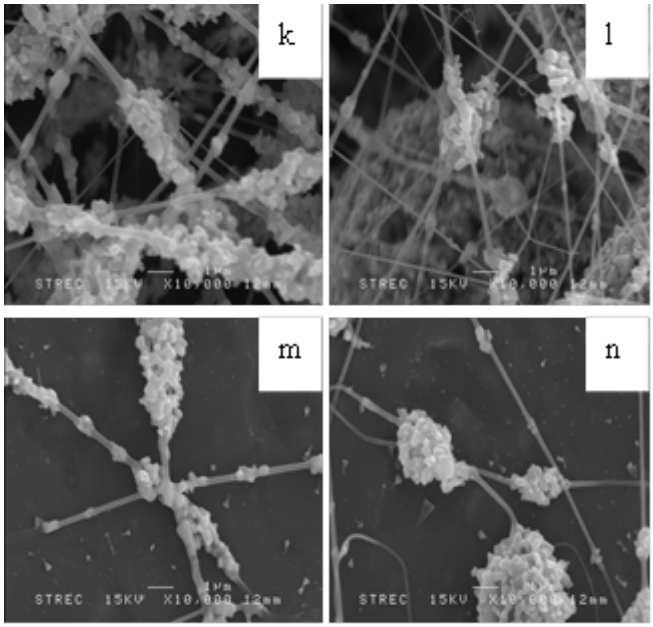

Fig.4.14 SEM micrographs of PVP/ZnO fibers which the weight percent of PVP to Ethanal equal to 10 weight percent, 17 kV applied electrical voltage and varying the weight ratios of PVP to ZnO 5:1 (a, b), 5:3 (c, d), 5:5 (e, f), 5:10(g, h), 5:20(i, j), 5:30(k, l), 5:50 (m,n) and using the method without dispersant (a c, e, g, I, k, m), with dispersant (b, d, f, h, j, l, n).

The morphology of PVP/ZnO nanofibers, which were fabricated at 10 weight percent of PVP in ethanol and the applied electrical voltage of 17kV and followed by ultrasonication without dispersant and with dispersant, showed variation of the weight ratio of PVP to ZnO. When the PVP/ZnO nanofibers had the minimum loading of ZnO, ZnO particles formed a few amount of node distribution as showed Fig4.14a, 4.14b. When the ZnO loading was increased, better distribution was obtained. ZnO particles were distributed with larger amount of node distribution.

When the loading of ZnO in PVP/ZnO fibers which had the weight ratios of PVP to ZnO equal to 5:10 resulted over crowed as shown in Fig 4.13g, 4.13h, the PVP/ZnO fibers formed uneven surface and ZnO particles were distributed in both nodes and fibers.

At the weight ratios of PVP to ZnO equal to 5:30, the fibers resulted over crowed accumulated particles with smaller fibers link age. ZnO particles mainly

distributed in nodes. Especially for the fibers with dispersant, some ZnO particles were distributed in nodes and some particles accumulated in large size diameter of about 9.60 μm. This typical nanofiber had smaller size diameter than that of the fibers without dispersant. The shape of nodes and accumulated particles in the fibers with dispersant were spherical and different from the fibers without dispersant. When the weight ratios of PVP to ZnO equal to 5:50, the broken fiber was obtained due to the PVP to ZnO ratio was over loading and fiber could not stand with the over stress in Fig4.14m, 4.14n.

The morphology of fiber fabrication with varying the weight ratios of PVP to ZnO was summarized in table 4.3

Table 4.3 Summary results of the fabrication of PVP/ZnO fibers

Condition		Actual weight ratios	The average diameter size		Fibers morphology
Theorical weight ratio	Dispersion method		Fibers	Nodes	
5:3(Fig4.14c)	without dispersant	5:1.60	248nm	599nm	Medium size diameter, ZnO particles mainly distributing in small nodes and fibers.
5:3(Fig4.14d)	with dispersant	5:1.74	252nm	486nm	Smaller size diameter and more ZnO particles distribution than without dispersant fibers at weight ratio 5:3. ZnO particles distributing in small nodes and fibers.
5:10(Fig4.14g)	without dispersant	5:9.84	274nm	777nm	Medium size diameter ZnO fairly distributing in both nodes and fiber.
5:10(Fig4.14h)	with dispersant	5:9.85	208nm	719nm	Smaller size diameter and more ZnO particles distribution than without

Condition		Actual weight ratios	The average diameter size		Fibers morphology
Theorical weight ratio	Dispersion method		Fibers	Nodes	
					dispersant fibers at weight ratio 5:10. ZnO particles fairly distributing in both nodes and fiber.
5:30(Fig4.13k)	without dispersant	5:23.12	211nm	681nm	Medium size diameter, ZnO particles distributing in accumulated particles the hold duct fibers
5:30(Fig4.13l)	with dispersant	5:24.38	156nm	689nm	Smaller size diameter than without dispersant fibers at weight ratio 5:30. ZnO particles mainly distri buting in nodes. **Some ZnO particles were accumulated in large size diameter about 9.60 µm.**

From SEM images in Fig 4.14m, 4.14n, the fiber broken would result from that the viscosity was increased suddenly in association with the formation of higher friction inside the needle when the loading capacity of ZnO value was over the maximum limitation (Fig.4.15)

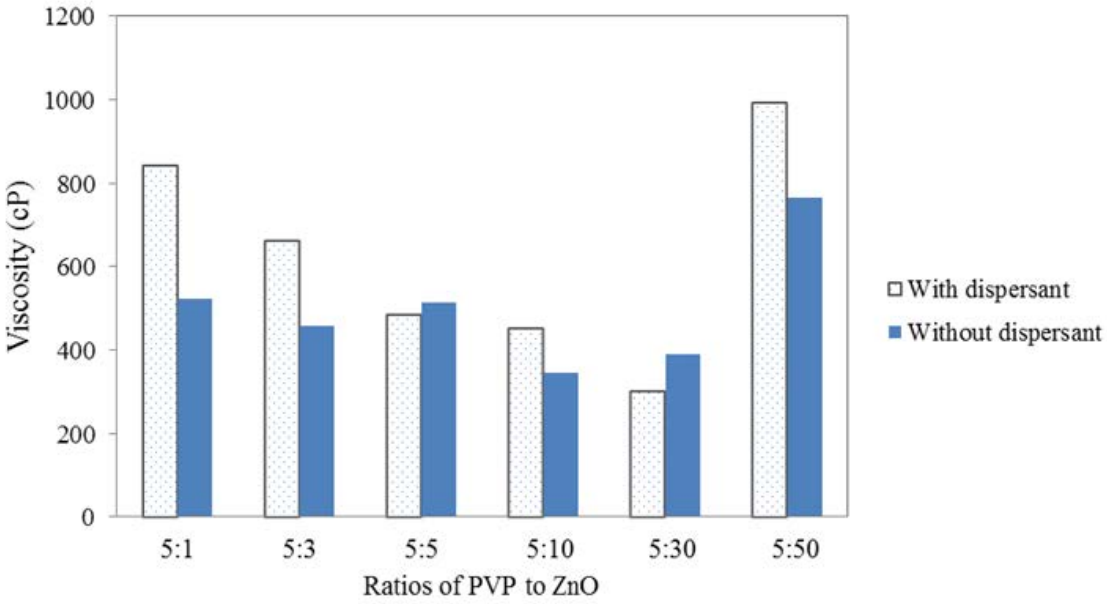

Fig.4.15 Relationship between viscosity and shear rate for polymer and composite polymer fluid

4.3 Photocatalytic degradation of Solid phase PVP

Photocatalytic activities could be effective to organic compound and solid-phase PVP degradation. This study is aimed to investigate the photocatalytic degradation of solid-phase PVP to understand its stability for VOC removal. The effect of morphology on stability of nanofibers would be analyzed and discussed.

4.3.1 Photocatalytic degradation of Solid phase PVP of PVP nanofibers

The fabricated PVP nanofibers are situated in a photo reactor to examine its stability for VOC removal. The photocatalytic degradation reactions of solid phase polymer were carried out under atmospheric condition in a reactor using UV-A as the irradiation sources for 48 hr. PVP fibers were prepared as a 20–30 mg rectangle mat with about 24 cm^2 area. The irradiation distance between the lamp and the sample was 10 cm. The exposure periods of UV light for the PVP nanofibers were 0, 1, 3, 6, 12, 24 and 48 hours. After the irradiation of the fibers was completed, the studied samples were weighed. Fig 4.16 showed the weight loss of PVP by a photo degradation. At the beginning, the weight of PVP fibers were gradually decreased

until 24 hr. and then they were dramatically fall. The weight remaining of PVP fibers after irradiation under UV-A source for 2 days were 58.14 % weight of PVP.

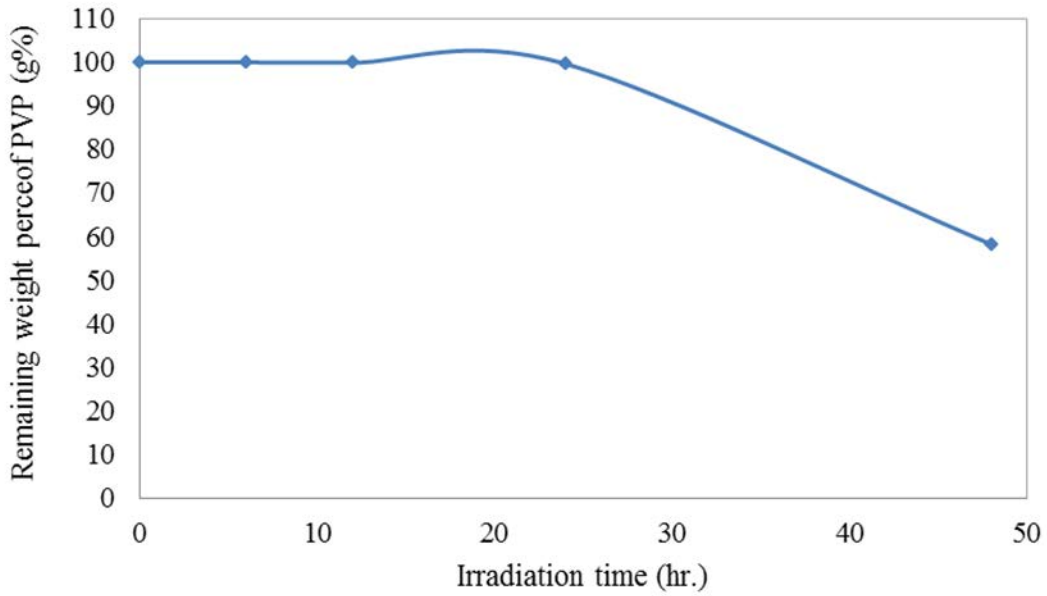

Fig.4.16 The weight losses of PVP by a photocatalytic reaction

The results from Fig 4.16 were consistent with SEM images of PVP nanofibers irradiated under UV-A light at different times as showed Fig. 4.17. The images showed that the fibers were deformed to produce film with in 24hr. the slowly decreasing of the weight of PVP were observed. After 24 hr. the fibers film were started decompose as shown in Fig. 4.17d leading to the fast decreasing of the weight of PVP.

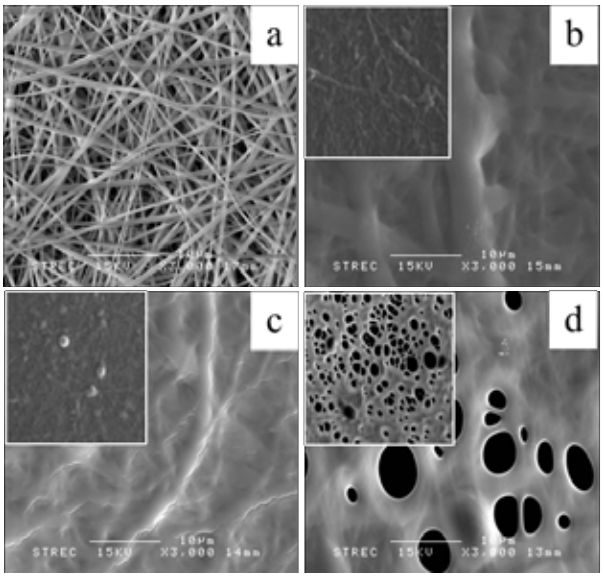

Figure 4.17 SEM micrographs of PVP nanofiber irradiated under UV-A light at different times a) 0 hr., b) 12hr., c) 24hr., and d) 48hr.

Gijsman et al. [17] suggested that the UV- degradation of polymer was due to the combined effects of photolysis and oxidative reactions. Sunlight photolytic degradation and/or photooxidation can only occur when the polymer contains chromophores which absorb wavelengths of the sunlight spectrum on earth (>290 nm). These wavelengths have sufficient energy to cause a dissociative (cleavage) process resulting in degradation.

Singh et al. [31] suggested the mechanisms of the degradation and oxidation reactions of the polymer which absorb light quanta and form excited states. Initially short-lived singlet state is transformed to long-lived triplet state. Excited triplet states may cleave the polymer chains and form radical pairs or form pairs of saturated and unsaturated chain ends by hydrogen transfer . The polymer radicals may add molecular oxygen to peroxy radicals, which abstract hydrogen and form hydroperoxide groups. Double bonds may add excited oxygen molecules in singlet state. In this reaction, the double bond is shifted to an adjacent C-C bond and a hydroperoxide group is formed. Some synthetic polymers, e.g. aromatic polyesters and polyamides, have inherent absorption of UV light, causing excitation, radical formation, oxygen addition, splitting off small molecules, chain scission, etc. Some of these polymers are auto-stabilized towards photodegradation by formation of an

oxidized surface layer with high absorption of near UV and visible light of short wavelengths, preventing further penetration of light into deeper layers [38].

Bhattacharya et al.[62] were found that increasing moisture content of the PVP film induces significant morphological changes in the polymer matrix, which affects both rotational and translational diffusion of single-molecule tracers. Upon exposure to low amounts of water vapor (RH of ~30%), the polymer network swells slightly to allow for rotational mobility of the probes residing therein, indicating onset of plasticization.

The deformation of PVP fibers could from both the UV degradation and the moisture content from environment due to the humidity was not controlled in this study.

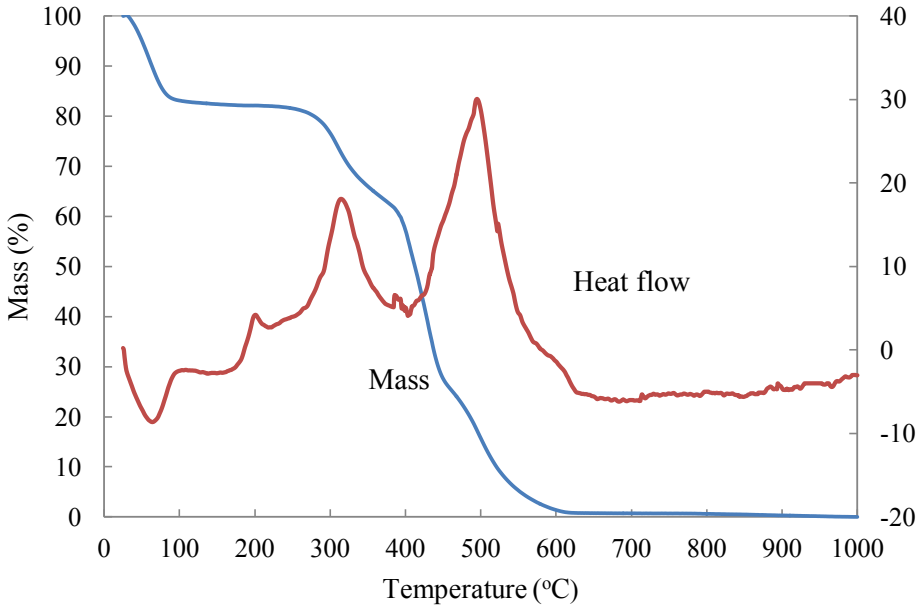

Figure 4.18 TGA/DSC curve of PVP electrospun fiber.

Fig4.18. represented the TGA/DSC curve of PVP fibers being heated up temperature in range of 25-1000 °C under oxygen gas having a flow rate of 40 ml/min. The blank PVP nanofibers show two significant steps of weight loss. The first weight loss of 20 percent was of the temperature ranging from 25 to 100 °C, which was related to the release of solvents and moisture from the sample[63]. The

second weight loss started at above 270 °C and finished at almost 600 °C, which was caused by the decomposition of the PVP polymer.The PVP nanofibers were totally decomposed.

There were exothermic events with peak located at 193°C, 306°C and exothermic maximum was obtained at 488°C. The peak located at 193°C that was nearly melting point of pure PVP about 150-180°C.

4.3.2 Photocatalytic degradation of Solid phase PVP of PVP/ZnO nanofibers

The fabricated PVP/ZnO nanofibers were situated in a photo reactor to examine its stability for VOC removal. The photocatalytic degradation reactions of solid phase polymer were carried out under atmospheric condition in a reactor using UV-A as the irradiation sources for 48 hr. PVP/ZnO fibers were prepared as a 20–30 mg rectangle mat with about 24 cm^2 area. The irradiation distance between the lamp and the sample was 10 cm. The exposure periods of UV light for the PVP nanofibers were 0, 1, 3, 6, 12, 24 and 48 hours. After the irradiation of the fibers was completed, the studied samples were employed by using thermogravimetric and differential thermal analyzer (TG/DTA) to examine weight ratios of PVP and ZnO on nanofibers before and after irradiation.

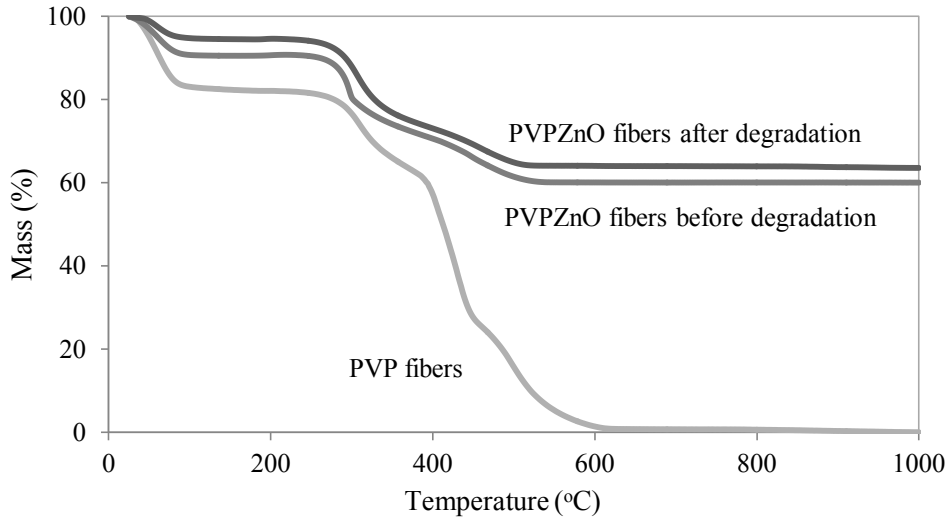

Figure 4.19 TGA curve of PVP fibers, PVPZnO fibers before and after degradation.

Fig.4.19 showed the TGA curve of PVP fibers, PVP/ZnO fibers before irradiation and PVPZnO fibers after irradiation for 48 hr. under UV-A source. All samples were fabricated at 10 weight percent of PVP in ethanol and the applied electrical voltage of 17kV followed by ultrasonication without dispersant. The fibers were heated up temperature in range 25-1000 °C under oxygen gas 40 ml/min. The three type fibers showed two significant steps of weight loss. The first weight loss was in the temperature ranging 25–100 °C, which is related to the release of solvents and moisture from the sample. The second weight loss started at above 270 °C and finishes at 600 °C.

The TGA curve of PVPZnO fibers before irradiation under UV-A resulted that the first solvents and moisture weight loss of 9.5% was obtained at the temperature of 25–100 °C. The second, the weight loss of PVP of 30.5% started at 280°C and finished at 550 °C. The remaining weight of 60% was ZnO particles which was decomposition at very high temperature of about1970-1975°C [11].

The TGA curve of PVP/ZnO fibers after irradiation under UV-A resulted that the first, solvents and moisture weight loss of 5.5% was obtained at the temperature range of 25–100 °C. The second, weight loss of PVP of 30.5% started at 280°C and finished at almost 550 °C. The remaining weight of 64% was ZnO particles.

In comparison with weight percent of PVP and ZnO in PVP/ZnO fibers before irradiation and PVP/ZnO fibers after irradiation under UV-A source, The weight percent of PVP in the fibers before irradiation was larger than that of the fibers after irradiation up to 33.7% and 25.82% respectively. The weight percent of ZnO in the fibers before irradiation was smaller than that of the fibers after irradiation up to 66.3% and 74.18% respectively.

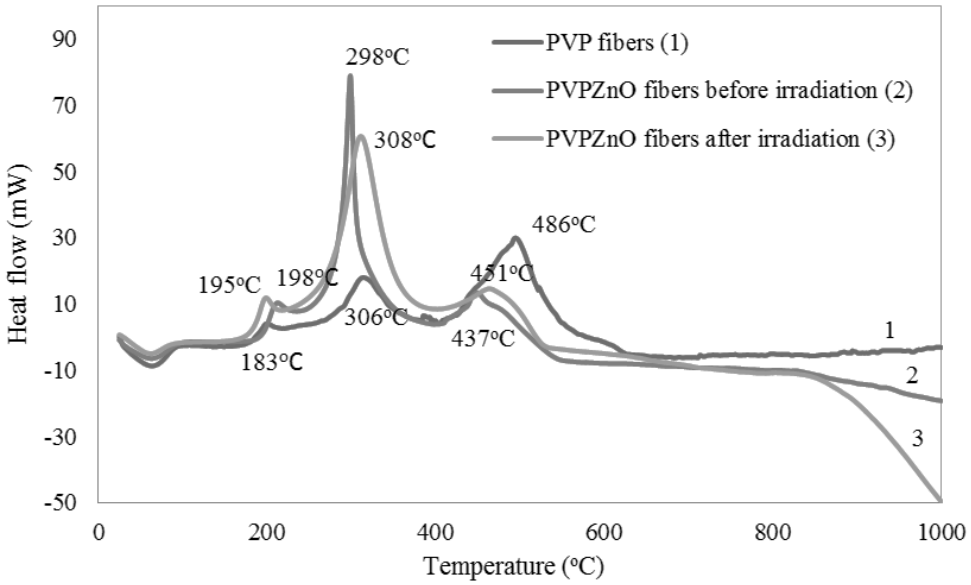

Figure 4.20 DSC curve of PVP fibers, PVPZnO fibers before and after degradation.

From DSC curve of all three samples in Fig 4.20, there were exothermic events with peak located at three parts. The first the exothermic peak of PVP fibers, PVP/ZnO before irradiation and PVP/ZnO fibers after irradiation were located at 183°C, 198°C and 195°C respectively. Second part of the exothermic peak of PVP fibers, PVP/ZnO before irradiation and PVP/ZnO fibers after irradiation were located at 306°C, 298°C and 308°C respectively the final exothermic peak of PVP fibers, PVP/ZnO before irradiation and PVP/ZnO fibers after irradiation were located at 486°C, 437°C and 451°C respectively.

4.3.2.1 Effect of The weight percent of PVP to Ethanol on the photodegrada tion efficiency

The samples which had different weight percent of PVP to ethanol were exposed to irradiation of UV-A light for 48 hr. in ambient air. Each sample was employed by using thermogravimetric and differential thermal analyzer (TG/DTA) to examine weight ratios of PVP and ZnO on nanofibers before and after irradiation. The weight loss of PVP by photocatalytic degradation was calculated as the function of irradiation time. The morphology was investigated by Electron microscopy.

The previous results in Fig.4.12 exhibited the effect of the weight percent of PVP to ethanol on the fibers morphology. When the concentration of PVP was

increased, fibers diameter was increased. In comparison of the distribution of ZnO particles imbedded in PVP polymer matrix, the larger size diameter fiber could be obtained with ZnO particles distributing in the hold fiber for 12 weight percent fibers. For small size diameter fiber, node distribution and non-uniformity were obtained from PVP/ZnO fibers at 8 weight percent fibers.

In Fig.4.21, the photodegradation efficiency was affected by the weight percent of PVP to ethanol. When all samples which fabricated at the weight ratios of PVP to ZnO 5:10, 17 kV applied voltage, having difference in the weight percent of PVP to ethanol were exposed to irradiation of UV-A light for 48 hr. in ambient air. In comparison of all weight percent of PVP to ethanol in this study, the maximum weight losses of 23.38% was obtained from the 10 weight percent fibers without dispersant. The minimum weight loss of 0.68 % was obtained from the 12 weight percent of PVP to Ethanol fibers without dispersant.

Fig.4.22 showed SEM micrographs of PVPZnO nanofiber without dispersant before and after irradiation under UV-A light for 48hr. at different weight percent of PVP to ethanol. After exposing to irradiation of UV-A light, the fibers were gradually deformed to film. Then the film was gradually decomposed. The remaining weight of PVP of the 8, 10 and 12 weight percent fibers resulted up to 97.96%, 76.72% and 99.32% respectively.

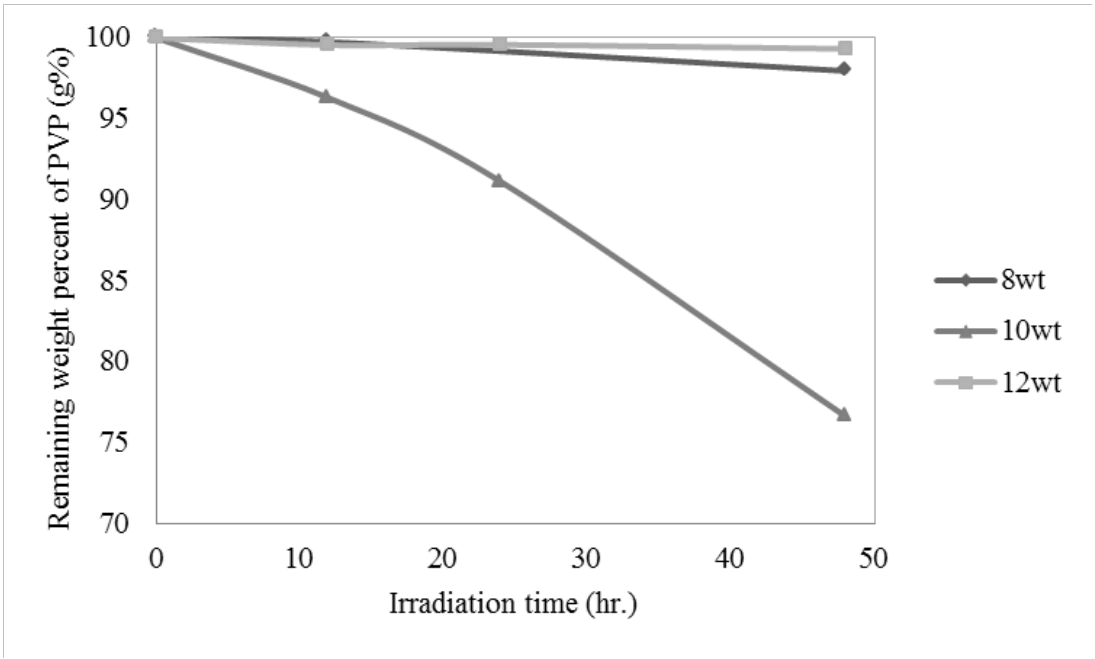

Fig. 4.21 The weight losses of PVP by a photocatalytic reaction

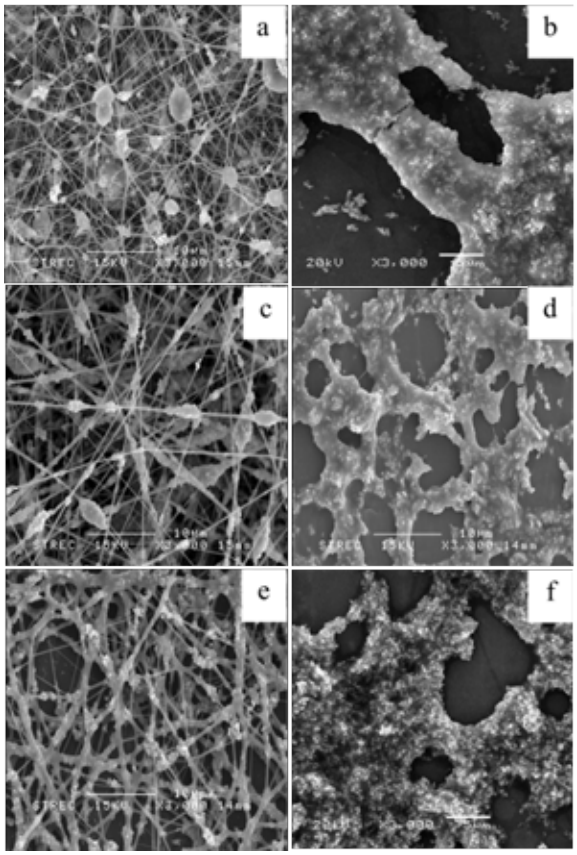

Fig. 4.22 SEM micrographs of PVPZnO nanofiber without dispersant a, c, e) before and b, d, f) after irradiation under UV-A light for 48hr. at different weight percent a, b) 8wt% c, d) 10 wt% e, f) 12wt%

For larger size fiber diameter from 12 weight percent fibers, the penetration of UV light into photocatalyst could be related to amount of the polymer used or the fibers diameter. The large amount of polymer in fiber composition could lead to thick of polymer coating on the ZnO particles. This coating could delay the penetration of UV spectra, resulting in lower degradation. For ZnO distribution, ZnO particles could be distributed in the hold fiber due to their large size diamerter. The ZnO particles could help decreasing the photodegradation efficiency of PVP due to the UV-A adsorbtion of ZnO particles. The fast degradation could obtained from the smaller fibers due to their smaller diameter of fibers and node distribution with non-uniformity of ZnO particles.

4.3.2.2 Effect of The applied voltage on the photodegradation efficiency

The samples which had prepare by different applied voltage were exposed to irradiation of UV-A light for 48 hr. in ambient air. Each sample was employed by using thermogravimetric and differential thermal analyzer (TG/DTA) to examine weight ratios of PVP and ZnO on nanofibers before and after irradiation. The weight loss of PVP by photocatalytic degradation was calculated as the function of irradiation time. The morphology was investigated by Electron microscopy.

Fig.4.10 and Fig.4.11 exhibited the effect of the applied voltage on the fibers morphology. The diameter of the nanofiber was smaller when the applied voltage was increased. In comparison of the distribution of ZnO particle imbedded in PVP polymer matrix, the big size diameter fiber could be obtained with ZnO particles distributing in the hold fiber. For small size diameter fiber, node distribution and non-uniformity were obtained from the 21 kV applied voltage fibers.

From Fig.4.23, the photodegradation efficiency was affected by the applied voltage. When all samples which fabricated at the weight ratios of PVP to ZnO 5:10, 10 weight percent of PVP to Ethanol, having difference in the applied voltage were exposed to irradiation of UV-A light for 48 hr. in ambient air. In comparison with all applied voltage in this study, the maximum weight losses of 23.38% were obtained from the 17 kV applied voltage fibers without dispersant. The minimum weight loss of 1.07 % was obtained from the 13 kV applied voltage fibers without dispersant.

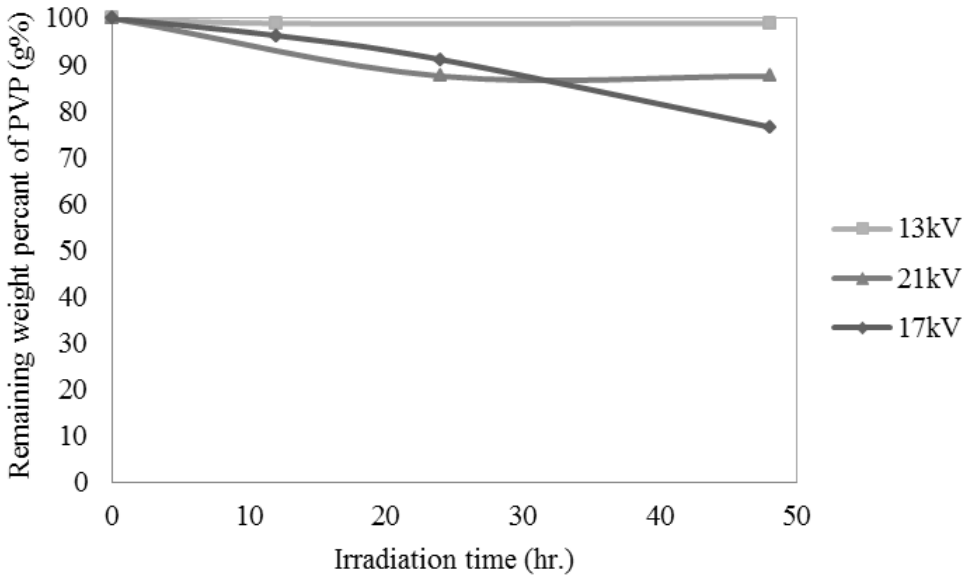

Fig. 4.23 The weight losses of PVP by a photocatalytic reaction

Fig.4.24 showed SEM micrographs of PVP/ZnO nanofiber without dispersant before and after irradiation under UV-A light for 48hr. at different applied voltage. After exposing to irradiation of UV-A light, the fibers were gradually deformed to film. Then the film was gradully decomposed. The remaining weight of PVP of the 13, 17 and 21 weight percent fibers resulted up to 98.93%, 76.72 % and 87.55% respectively.

The results were consistent with the results of the weight percent of PVP to ethanol on the photodegradation efficiency. The larger size diamerter fiber were obtained from 13 kV applied voltage and the results revealed lower degradation due to the larger fibers diamerter could lead to thick of polymer coating on the ZnO particles. This could delay the penetration of UV spectra. And ZnO particles could be distributed in the hold fiber due to their large size diamerter. The ZnO particles could help decreasing the photodegradation efficiency of PVP due to the UV-A adsorbtion of ZnO particles. While the smaller fibers were fast degradation due to their smaller diameter of fibers and node distribution with non-uniformity of ZnO particles as Fig 4.24.

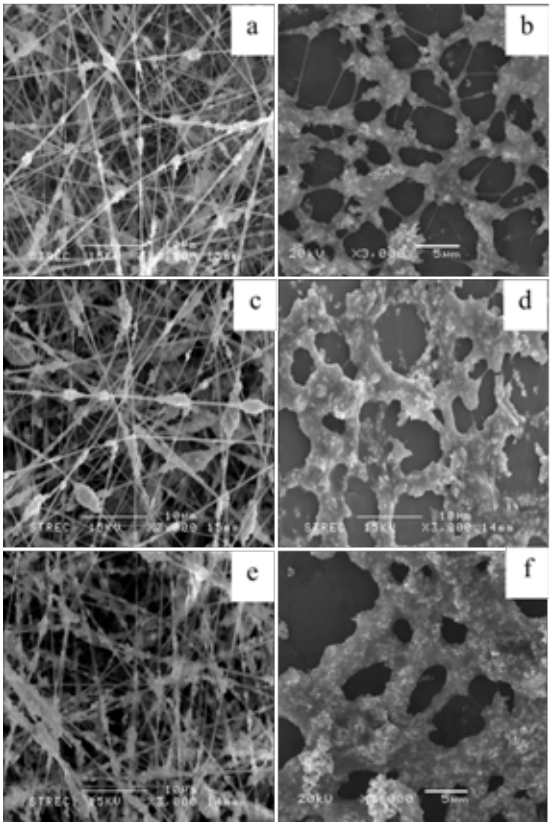

Fig.4.24 SEM micrographs of ZnO/PVP nanofiber a, c, e) before and b, d, f) after irradiation under UV-A light at different applied voltage a, b) 13kV c, d) 17kV e,f) 21kV

From the results, the fibers morphology was affected to the photodegradation efficiency and the stability of the fibers. From all samples, the PVP/ZnO fibers which were fabricated at the weight ratios of PVP to ZnO 5:10, 13 kV applied voltage, by the 12 weight percent of PVP to ethanol were the most stable fibers for this studies.

4.3.2.3 Effect of weight ratio of PVP to ZnO on the photodegradation efficiency

The samples which had difference in the weight ratios of PVP to ZnO were exposed to irradiation of UV-A light for 48 hr. in ambient air. Each sample was employed by using thermogravimetric and differential thermal analyzer (TG/DTA) to examine weight ratios of PVP and ZnO on nanofibers before and after irradiation. The weight loss of PVP by photocatalytic degradation was calculated as the function of irradiation time. The morphology was investigated by Electron microscopy.

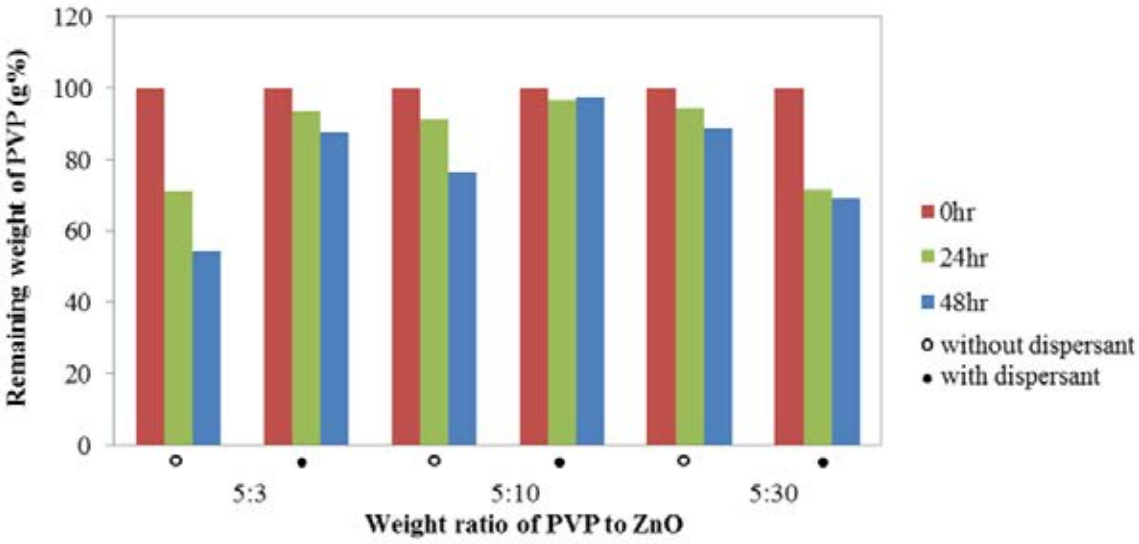

Fig. 4.25 The weight losses of PVP by a photocatalytic reaction

In Fig.4.25, the photodegradation efficiency was affected by the weight ratio of PVP to ZnO and the dispersion method when all samples, having difference in the weight ratio of PVP to ZnO were exposed to irradiation of UV-A light for 48 hr. in ambient air. In comparison of all weight ratio PVP to ZnO in this study, the maximum weight losses of 45.74% was obtained from the fibers without dispersant weight ratio PVP to ZnO 5:3 which larger than that of PVP fibers of 41.86% in Fig.4.18. The minimum weight loss of 2.61 % was obtained from the PVP/ZnO fibers with dispersant weight ratio PVP to ZnO 5:10.

In comparison of all weight ratio PVP to ZnO in this study, the fibers morphology in Fig.4.26, Fig.4.27 and Fig.4.28 were exhibited the fibers degradation. Fast degradation could be observed in the area of low density of fibers while slower degradation was derived from high density area. High dense area of fibers showed that the fibers were deformed to film.

The weight ratio PVP to ZnO 5:3 fibers as shown in Fig.4.26 were gradually deformed to film and total deformation was obtained after exposing to irradiation of UV-A light for 48hr. The remaining weight of PVP from the fiber with dispersant was larger than that of the fibers without dispersant up to 87.73% and 54.26% respectively.

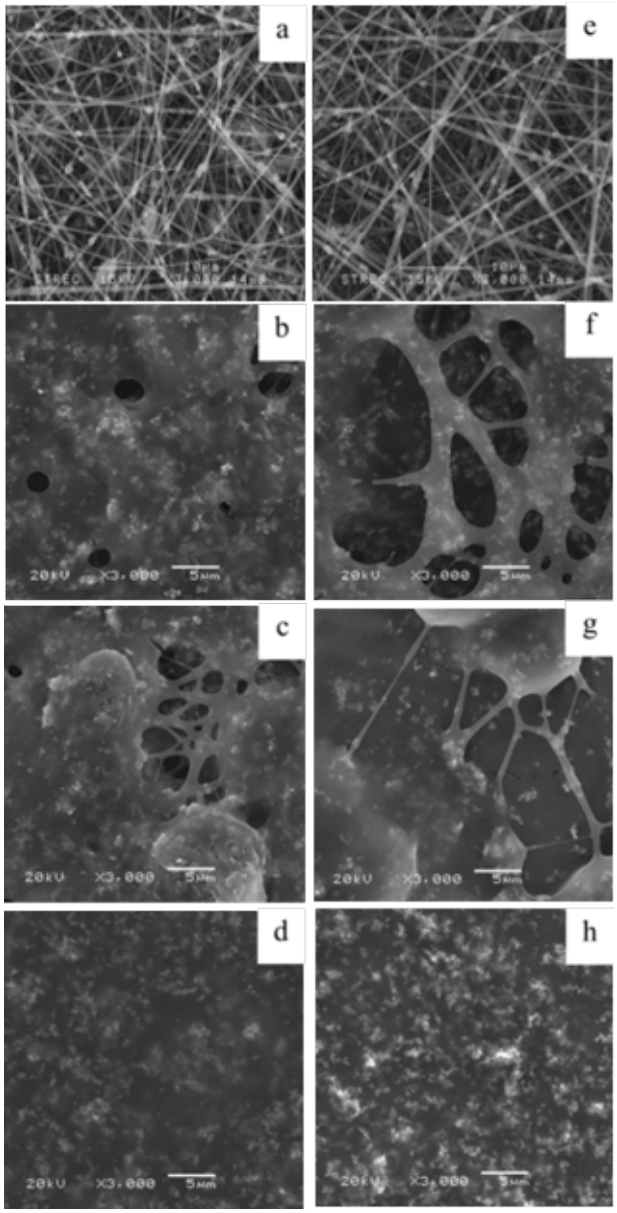

Fig. 4.26 SEM micrographs of PVPZnO nanofiber which were fabricated at the weight ratios of PVP to ZnO 5:3,10 weight percent of PVP in Ethanol and difference dispersion method, a, b, c, d) without dispersant and e, f, g, h) with dispersant, irradiated under UV-A light at different times a, e) 0 hr., b, f) 12hr., c, g) 24hr., and d, h) 48hr.

Fig.4.27 showed SEM images of the weight ratio of PVP to ZnO equivalent to 5:10. After exposing to irradiation of UV-A light, the fibers were gradually deformed to film. Then the film was gradually decomposed. The remaining weight

of PVP of the fibers with dispersant resulted up to 97.39% whereas the fibers without dispersant was 76.62%.

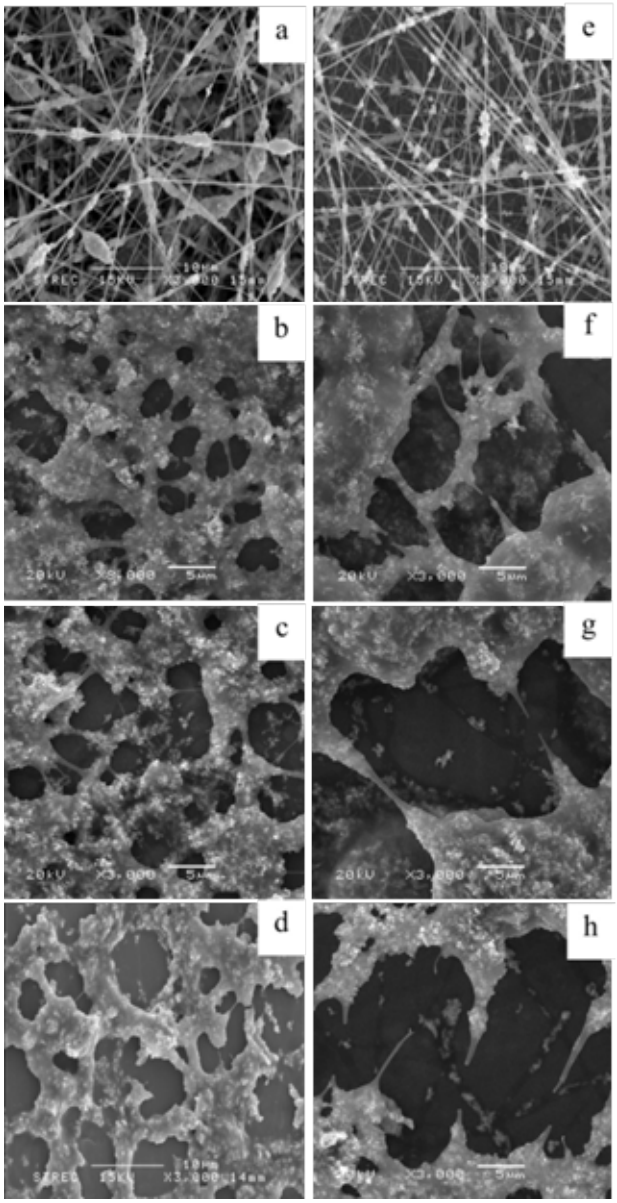

Fig. 4.27 SEM micrographs of PVPZnO nanofiber which were fabricated at the weight ratios of PVP to ZnO 5:10., 10 weight percent of PVP in Ethanol and difference dispersion method, a, b, c, d) without dispersant and e, f, g, h) with dispersant, irradiated under UV-A light at different times a, e) 0 hr., b, f) 12hr., c, g) 24hr., and d, h) 48hr.

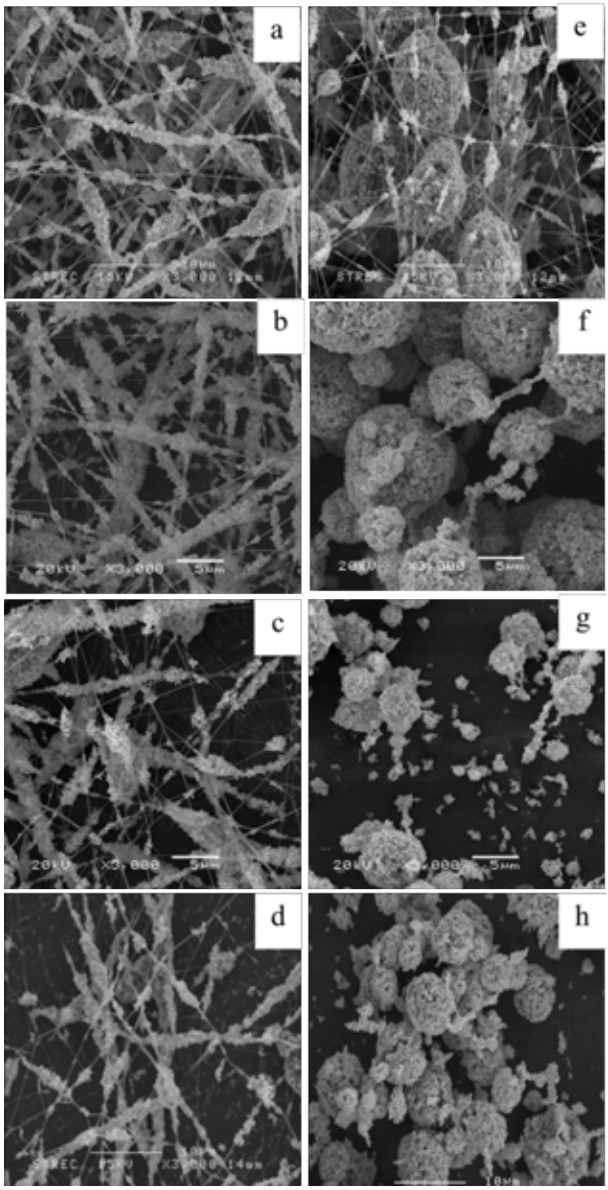

Fig. 4.28 SEM micrographs of PVPZnO nanofiber which were fabricated at the weight ratios of PVP to ZnO 5:30., 10 weight percent of PVP in Ethanol and difference dispersion method, a, b, c, d) without dispersant and e, f, g, h) with dispersant, irradiated under UV-A light at different times a, e) 0 hr., b, f) 12hr., c, g) 24hr., and d, h) 48hr.

The fibers web obtained from the weight ratio of PVP to ZnO 5:30 in Fig.4.28 resulted over crowed particles after the samples were irradiated to UV-A light for 48hr. Fibers were deformed to remain particles with smaller fibers linkage.

Especially, the fibers with dispersant were fast degradation due to their smaller size fibers than that of fibers without dispersant and node distribution. The weight of PVP remained in the fibers with dispersant lower than that of the fibers without dispersant up to 68.8% and 88.7% respectively.

As showed in Fig.4.25, the remaining weight of PVP in the fibers with dispersant was more than the fibers without dispersant in the weight ratio PVP to ZnO 5:3 and 5:10. The analytical data resulting in Fig.4.32 would suggest that the sample added with sodium hexametaphosphate exhibited some distinctive peaks near 1030 nm. It probably derived from the dispersant leading to decrease photocatalytic activities. For the weight ratio PVP to ZnO 5:30, the result showed the remaining weight of PVP in the fibers with dispersant was less than the fibers without dispersant due to their larger accumulated ZnO particles on sample, leading to decreasing the surface area of ZnO particles.

The weight loss of PVP of the PVP/ZnO fibers in the weight ratios PVP to ZnO 5:10 was smaller than that of the fibers in the weight ratios PVP to ZnO 5:3. It was indicated that the ZnO particles could help decreasing the photodegradation efficiency of PVP due to the UV-A adsorbtion of ZnO particles. The weight loss of PVP of the PVPZnO fibers in the weight ratios PVP to ZnO 5:30 was larger than that of the fibers in the weight ratios PVP to ZnO 5:10. It could be obtained from over loading of ZnO of the fibers in the weight ratios PVP to ZnO 5:30. The fibers resulted over crowed accumulation of particles with smaller fibers linkage. Especially the fibers with dispersant, some ZnO particles were distributed in nodes and some particles accumulated in a large spherical form with diameter size of about 9.60 μm. The photodegradation efficiency of the fibers without dispersant in the weight ratios PVP to ZnO 5:30 were stable than that of the fibers with dispersant in the weight ratios PVP to ZnO 5:30.

Yang et al.[64] studied the mechanisms of TiO2 as UV-blocking Additive for Films. When the TiO_2 is illuminated by light with energy higher than its band gaps, the electrons will absorb the energy of the photons and be excited to cross the band gap, so as to produce the pairs of electrons and holes. These excited electrons

and holes will then result in two competing consequences: either combing with other holes or electrons, or being captured by the absorbents surrounding TiO_2 and initiating reduction and oxidation reactions.

4.3.3 Spectroscopic evidence of degradation

4.3.3.1 The spectroscopic evidence of PVP degradation of PVP fibers

The FT-IR spectra of the original PVP fibers irradiated by UV-A for different time were showed in Fig.4.29. The IR spectra of 3430 cm^{-1}, 2955 cm^{-1}, 1656cm^{-1}, 1440cm^{-1}, 1229 cm^{-1} and 650 cm^{-1} could result in relation with O-H, C-H, C=C ring, CH_2, C-N and C-C peaks, respectively when the PVP had no irradiation time [14].

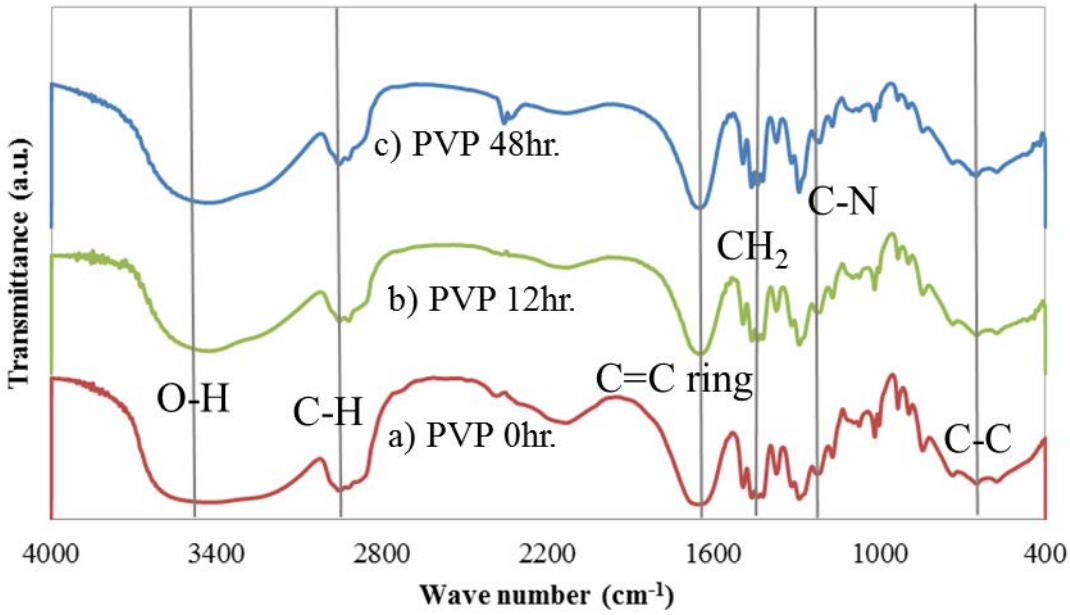

Fig.4.29 FTIR spectra of PVP fibers irradiated by UV-A at a) 0hr, b)12hr, c)48hr.

It could be observed that the intensity ratios of the characteristics of PVP were not clearly changed with the irradiation time. After UV-A irradiation for 48 hr. C-N peak was shifted from 1229 cm^{-1} to 1218 cm^{-1}. While the peak C=C ring and CH_2 became narrow.

Kharroubi et al. [65] suggested that the IR broad peak in the range of 3200–3600cm^{-1} could correspond to OH stretching, and peaks about 2900 cm−1 indicating to C–H stretching. The two principal peaks were observed between 1400 and 1650

cm^{-1}, corresponding to the symmetric and asymmetricstretching of the carboxyl group (C=O). The band in the range of 400–550 cm^{-1} could relate to the Zn–O stretching mode. The O–H stretching at 2550 cm^{-1} and O–H about 1650–1750 cm^{-1}, suggesting that moisture was adsorbed in the samples. The peaks were observed ordinarily between 2300 and 2400 cm^{-1} due to adsorbed CO_2 molecules in air [66].

4.3.3.2 The spectroscopic evidence of PVP degradation of PVPZnO fibers without dispersant

After the samples were exposed to irradiation of UV-A light for 48 hr. in ambient air. The FT-IR spectra of the PVP/ZnO fibers without dispersant irradiated by UV-A for different time were showed in Fig.4.30. The FT-IR spectra of the samples showed overlap between the spectra of PVP and ZnO. The IR spectra of 3425 cm^{-1}, 2954 cm^{-1}, 1654cm^{-1}, 1440cm^{-1}, 1229 cm^{-1} and 450 cm^{-1} could result in relation with O-H, C-H, C=C ring, CH_2, C-N, C-C and Zn-O peaks, respectively when the fibers had no irradiation time as showed Fig.4.31 (a).

After the samples were exposed to irradiation of UV-A light for 48 hr. in ambient air as shown in Fig 4.30. The result showed that the C-H peak of 2954 cm^{-1} on IR spectra could shift to 2923 cm^{-1}.When the sample was employed by using Thermogravimetric and differential thermal analyzer (TG/DTA) in Fig 4.30 (d). It found that the spectra after employing by TGA/DSC was similar with the IR spectra of ZnO particles without dispersant. Zn-O peak of 450cm^{-1} was clearly observed.

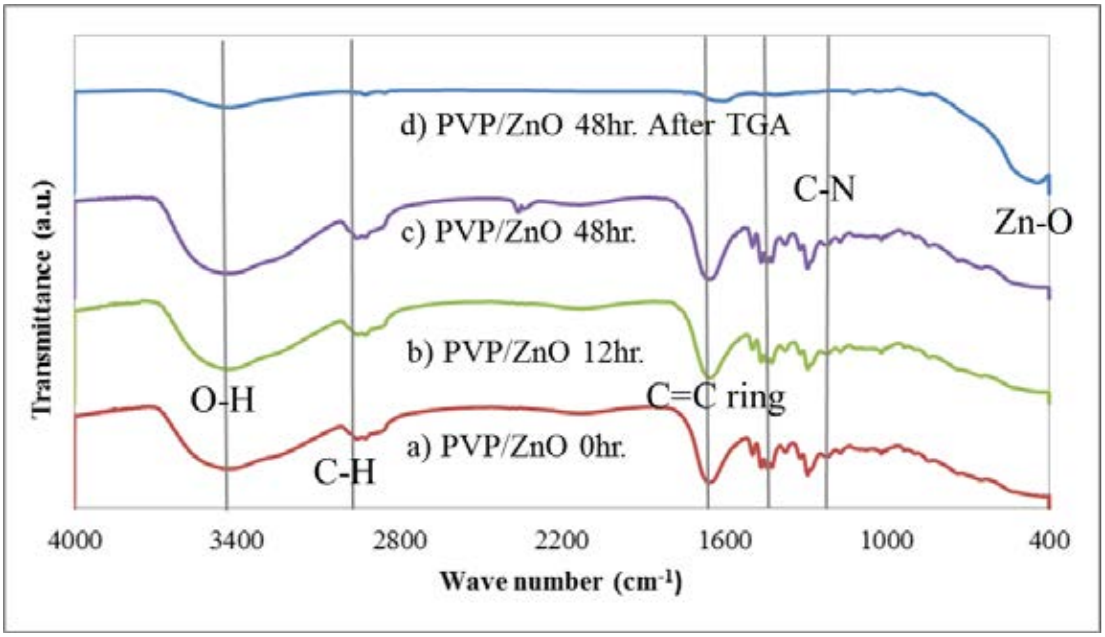

Fig.4.30 FTIR spectra of PVPZnO fibers without dispersant irradiated by UV-A at (a) 0hr, (b)12hr, (c)48hr and 48hr irradiation sample after calcination 1000 ^{o}C by using TGA/DSC

4.3.3.3 The spectroscopic evidence of PVP degradation of PVP/ZnO fibers with dispersant

After the samples were exposed to irradiation of UV-A light for 48 hr. in ambient air. The FT-IR spectra of the PVP/ZnO fibers with dispersant irradiated by UV-A for different time were showed in Fig.4.31. The FT-IR spectra of the samples showed overlap between the spectra of PVP, ZnO and dispersant. The IR spectra of 3425 cm^{-1}, 2953 cm^{-1}, 1652cm^{-1}, 1440cm^{-1}, 1229 cm^{-1} and 450 cm^{-1} could result in relation with O-H, C-H, C=C ring, CH_2, C-N, C-C and Zn-O peaks, respectively when the fibers had no irradiation time as showed Fig.4.31 (a).

After the samples were exposed to irradiation of UV-A light for 48 hr. in ambient air as shown in Fig 4.32. The result showed that the C-H peak of 2953 cm^{-1} on IR spectra could shift to 2924 cm^{-1}.When the sample was employed by using Thermogravimetric and differential thermal analyzer (TG/DTA) in Fig 4.31 (d). It found that the spectra after employing by TGA/DSC was similar with the IR spectra of ZnO particles with dispersant. Zn-O peak of 450cm^{-1} and P-O peak of 1055 cm^{-1}

were clearly observed. It confirmed that the dispersant was not decompose after UV irradiation and calcination at high temperature.

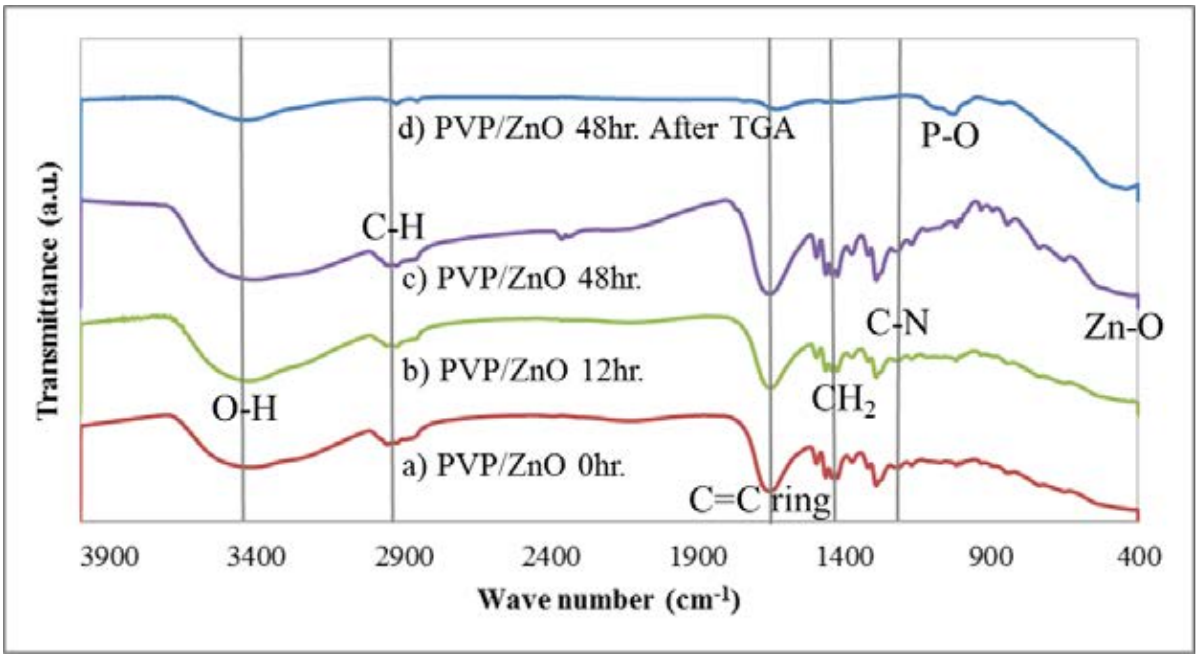

Fig.4.31 FTIR spectra of PVPZnO fibers with dispersant irradiated by UV-A at a) 0hr, b)12hr, c)48hr and d) 48hr irradiation sample after calcination 1000^{o}C by using TGA/DSC

He et al. [30] suggested that after the UV irradiation, the characteristics of photocatalyst would increase and polymer would decrease with the increasing irradiaton time due to the degradation of PVP in the composition sample.

CHAPTER V

CONCLUSION AND RECOMMENDATIONS

5.1 Summary of the results

1. ZnO particles imbedded in PVP polymer matrix could favorably be fabricated by using direct-dispersed processing and electrospinning method.

2. Size and morphology of fibers were manipulated by adjusting on weight ratio of PVP to ZnO, weight percent of PVP in ethanol, operating applied voltage in electrospinning process.

3. In this work, the diameter of fibers could be tuned by the weight percent of PVP to Ethanol and the supply voltage. When the concentration of PVP was increased, the bigger fiber diameter in size was obtained. While the supply voltage was increased, the smaller fibers were obtained.

4. For the dispersion of ZnO on the fibers, the results would suggest that better dispersion of ZnO could be improved by the synergetic effect of ultrasonic cavitation and sodium hexametaphosphate dispersant. The distribution of ZnO on fibers could be tuned by the diameter of fibers and the weight ratios of PVP to ZnO.

5. The PVP/ZnO fibers could be fabricated at high the weight ratios of PVP to ZnO up to 5:50. Broken fiber were obtained when the PVP to ZnO ratio was over loading and fiber could not stand with the over stress.

6. The irradiation UV-A could be effective to organic compound and solid-phase PVP degradation. The PVP nanofibers showed two significant steps of deformation. Firstly, the fibers were slowly deformed to film. In the second stage, the fibers film started to decompose, leading to the fast decreasing of 58.14% of the weight of PVP.

7. For the PVP/ZnO fibers degradation, the high ratios of PVP to ZnO fibers showed more stability of fibers than that of the small ratios of PVP to ZnO fibers. Due to ZnO particles could help decreasing the photodegradation efficiency of PVP due to the UV-A adsorbtion of ZnO particles.

8. The effect of dispersant on the photocatalytic activity showed that the dispersant on the fibers could decrease photocatalytic activities.

9. The photodegradation efficiency of the PVP/ZnO fibers was reduced with an increasing fiber diameter by tunning the weight percent of polymer or the supply voltage and increasing the dispersion of ZnO particles.

10. The most stable fibers in this study was obtained from the PVP/ZnO fibers which were fabricated at the weight ratios of PVP to ZnO 5:10, 13 kV applied voltage, by the 12 weight percent of PVP to Ethanol.

5.2 Conclusion

ZnO particles imbedded in PVP polymer matrix could be fabricated by using direct-dispersed processing and electrospinning method. Size and morphology of fibers were manipulated by adjusting on weight ratio of PVP to ZnO, percent weights of PVP in ethanol and operating applied voltage as parameters in electrospinning process. Effect of ultrasonic dispersion and dispersant on the uniformity of ZnO in PVP matrix showed better microstructure uniformity. The fabricated PVP-ZnO nanofibers were situated in a photo reactor to examine its stability for VOC removal. The result showed that the photodegradation efficiency was affected by the weight ratio of PVP to ZnO, the dispersion addition and the fibers diameter. In this study, the most stable fiber was obtained from the PVP/ZnO fibers which were fabricated at the weight ratios of PVP to ZnO 5:10, 13 kV applied voltage, by the 12 weight percent of PVP to Ethanol.

5.3 Recommendations for the future work

There are some recommendation for future studies given below.

1. Effect of some environment paramerters in experimental room such as humidity and temperature should be studied.

2. The degradation of PVP fibers under UV should be confirmed by exposing fibers under N_2.

3. The degradation of PVP/ZnO fibers under UV should be confirmed by exposing fibers under N2 due to the photodegradation of ZnO needs O_2.

REFERENCES

[1] Mo, J., et al., Photocatalytic purification of volatile organic compounds in indoor air: A literature review. Atmospheric Environment. 43(14) (2009): 2229-2246.

[2] Services, U.S.D.o.H.a.H. Public Health ServiceThe 12th Report on Carcinogens. Formaldehyde 2012; Available from: http://ntp.niehs.nih.gov/go/9732

[3] Tompkins, D.T., Evaluation of photocatalytic air cleaning capability: a literature review and engineering analysis. ASHARE Research Project RP. (2001): 1134.

[4] Pal, B. and M. Sharon, Enhanced photocatalytic activity of highly porous ZnO thin films prepared by sol–gel process. Materials Chemistry and Physics. 76(1) (2002): 82-87.

[5] Li, D. and H. Haneda, Morphologies of zinc oxide particles and their effects on photocatalysis. Chemosphere. 51(2) (2003): 129-137.

[6] Chakrabarti, S. and B.K. Dutta, Photocatalytic degradation of model textile dyes in wastewater using ZnO as semiconductor catalyst. Journal of Hazardous Materials. 112(3) (2004): 269-278.

[7] Yang, J.L., An, S. J., Park, W. I., Yi, G.-C. and Choi, W. , Photocatalysis Using ZnO Thin Films and Nanoneedles Grown by Metal–Organic Chemical Vapor Deposition. Adv. Mater. 16 (2004): 1661-1664.

[8] Sangkhaprom, N., P. Supaphol, and V. Pavarajarn, Fibrous zinc oxide prepared by combined electrospinning and solvothermal techniques. Ceramics International. 36(1) (2010): 357-363.

[9] Laforgue, A. and L. Robitaille, Fabrication of poly-3-hexylthiophene/polyethylene oxide nanofibers using electrospinning. Synthetic Metals. 158(14) (2008): 577-584.

[10] Chung, S.J., et al., Characterization of ZnO nanoparticle suspension in water: Effectiveness of ultrasonic dispersion. Powder Technology. 194(1–2) (2009): 75-80.

[11] Morkoç, H. and Ü. Özgür, Index, in *Zinc Oxide*. 2009, Wiley-VCH Verlag GmbH & Co. KGaA. p. 469-477.

[12] Moezzi, A., A.M. McDonagh, and M.B. Cortie, Zinc oxide particles: Synthesis, properties and applications. Chemical Engineering Journal. 185–186(0) (2012): 1-22.

[13] Watthanaarun, J., V. Pavarajarn, and P. Supaphol, Titanium (IV) oxide nanofibers by combined solgel and electrospinning techniques: preliminary report on effects of preparation conditions and secondary metal dopant. Science and Technology of Advanced Materials. 6(34) (2005): 240-245.

[14] Giri N. , N.R.K., Gunasekaran S., Shreemathi S. , NMR and FTIR spectroscopic study of blend behavior of PVP

and nano silver particles. Achives of Applied Science Research. 2011(3) (2011): 624-630.

[15] Park, J.-A., et al., Fabrication and characterization of ZnO nanofibers by electrospinning. Current Applied Physics. 9(3, Supplement) (2009): S210-S212.

[16] Reneker, D.H. and A.L. Yarin, Electrospinning jets and polymer nanofibers. Polymer. 49(10) (2008): 2387-2425.

[17] Gijsman, P., G. Meijers, and G. Vitarelli, Comparison of the UV-degradation chemistry of polypropylene, polyethylene, polyamide 6 and polybutylene terephthalate. Polymer Degradation and Stability. 65(3) (1999): 433-441.

[18] Chew, S.Y., et al., The role of electrospinning in the emerging field of nanomedicine. Current Pharmaceutical Design. 12(36) (2006): 4751-4770.

[19] Kidoaki, S., I.K. Kwon, and T. Matsuda, Mesoscopic spatial designs of nano- and microfiber meshes for tissue-engineering matrix and scaffold based on newly devised multilayering and mixing electrospinning techniques. Biomaterials. 26(1) (2005): 37-46.

[20] Stankus, J.J., et al., Microintegrating smooth muscle cells into a biodegradable, elastomeric fiber matrix. Biomaterials. 27(5) (2006): 735-744.

[21] Bhardwaj, N. and S.C. Kundu, Electrospinning: A fascinating fiber fabrication technique. Biotechnology Advances. 28(3) (2010): 325-347.

[22] Taylor, G., Disintegration of water drops in an electric field. Proceedings of the Royal Society of London. Series A, Mathematical and Physical Sciences. 97 (1964): 280-383.

[23] Taylor, G., Electrically driven jets. Proceedings of the Royal Society of London Series A, Mathematical and Physical Sciences. 75 (1969.): 313-453.

[24] Thompson, C.J., et al., Effects of parameters on nanofiber diameter determined from electrospinning model. Polymer. 48(23) (2007): 6913-6922.

[25] Yun, K.M., et al., Nanoparticle filtration by electrospun polymer fibers. Chemical Engineering Science. 62(17) (2007): 4751-4759.

[26] Li, D. and Y. Xia, Electrospinning of nanofibers: Reinventing the wheel? Advanced Materials. 16(14) (2004): 1151-1170.

[27] Sigmund, W., et al., Processing and structure relationships in electrospinning of ceramic fiber systems. Journal of the American Ceramic Society. 89(2) (2006): 395-407.

[28] Zhang, C., et al., Silver nanoparticles grown on the surface of PAN nanofiber: Preparation, characterization and catalytic performance. Colloids and Surfaces A: Physicochemical and Engineering Aspects. 362(13) 58-64.

[29] Wang, S., et al., Introducing CTAB into CdTe/PVP nanofibers enhances the photoluminescence intensity of CdTe nanoparticles. Materials Letters. 61(25) (2007): 4674-4678.

[30] He, C.-H. and J. Gong, The preparation of PVA–Pt/TiO2 composite nanofiber aggregate and the photocatalytic degradation of solid-phase polyvinyl alcohol. Polymer Degradation and Stability. 81(1) (2003): 117-124.

[31] Singh, B. and N. Sharma, Mechanistic implications of plastic degradation. Polymer Degradation and Stability. 93(3) (2008): 561-584.

[32] Platzer, N., Encyclopedia of Polymer Science and Engineering, H. F. Mark, N. M. Bikales, C. G. Overberger, and G. Menges, Wiley-Interscience, New York, 1985, 720 pp. Journal of Polymer Science Part C: Polymer Letters. 24(7) (1986): 359-360.

[33] Marek, A., et al., Spatial resolution of degradation in stabilized polystyrene and polypropylene plaques exposed to accelerated photodegradation or heat aging. Polymer Degradation and Stability. 91(3) (2006): 444-458.

[34] Hamid, S. and W. Prichard, Mathematical modeling of weather-induced degradation of polymer properties. Journal of applied polymer science. 43(4) (1991): 651-678.

[35] Turro, N.J., Modern molecular photochemistry. 1991: University Science Books.

[36] Otsu, T., H. Tanaka, and H. Wasaki, Photodegradation of chloromethyl vinyl ketone polymer and copolymers with styrene and α-methylstyrene. Polymer. 20(1) (1979): 55-58.

[37] Carlsson, D. and D. Wiles, The photooxidative degradation of polypropylene. Part I. Photooxidation and photoinitiation processes. Journal of Macromolecular Science—Reviews in Macromolecular Chemistry. 14(1) (1976): 65-106.

[38] Ravve A., Organic chemistry of macromolecules. an introductory textbook, ed. M. Dekker. 1967.

[39] Plotnikov VG., Effect of mechanical stresses on photochemical degradation of polymeric molecules. Dokl Akad Nauk SSSR. (301) (1988): 376-379.

[40] Gugumus F., In: Zweifel H, editor. Plastics additives handbook. 5th ed. Cincinnati: Hanser. 2001.

[41] Hocking, P.J., The classification, preparation, and utility of degradable polymers. Journal of Macromolecular Science, Part C: Polymer Reviews. 32(1) (1992): 35-54.

[42] Denisov, E., Developments in polymer stabilizaton. Applied Science. 5 (1982): 23-40.

[43] Carlsson, D.J. and D.M. Wiles, The Photooxidative Degradation of Polypropylene. Part I. Photooxidation and Photoinitiation Processes. Journal of Macromolecular Science, Part C. 14(1) (1976): 65-106.

[44] Rabek, J.F., Photostabilization of polymers: principles and applications. 1990: Elsevier applied science.

[45] Ginhac, J.M., et al., Influence of hydroperoxides on the photothermal oxidation of polyethylene. Die Makromolekulare Chemie. 182(4) (1981): 1017-1025.

[46] Arnaud, R., J.Y. Moisan, and J. Lemaire, Primary hydroperoxidation in low-density polyethylene. Macromolecules. 17(3) (1984): 332-336.

[47] Gugumus, F. *Some aspects of polyethylene photooxidation*. in *Makromolekulare Chemie. Macromolecular Symposia*. 1989. Wiley Online Library.

[48] Geuskens, G., et al., New aspects of the photooxidation of polyolefins. Polymer photochemistry. 5(1) (1984): 313-331.

[49] Geuskens, G. and M.S. Kabamba, Photo-oxidation of polymers: Part IX Additional comments about a new chain scission mechanism in polyolefins. Polymer Degradation and Stability. 5(5) (1983): 399-401.

[50] Gugumus, F., R. Gaechter, and H. Mueller, Plastics additives. Hanser Publishers, Munich, Germany. (1990): 129.

[51] Russell, G.A., Deuterium-isotope Effects in the Autoxidation of Aralkyl Hydrocarbons. Mechanism of the Interaction of PEroxy Radicals1. Journal of the American Chemical Society. 79(14) (1957): 3871-3877.

[52] Ohtani, B., Preparing articles on photocatalysis - beyond the illusions, misconceptions, and speculation. Chemistry Letters. 37(3) (2008): 217-229.

[53] Liqiang, J., et al., Deactivation and regeneration of ZnO and TiO2 nanoparticles in the gas phase photocatalytic oxidation of n-C7H16 or SO2. Applied Catalysis A: General. 275(1-2) (2004): 49-54.

[54] Liao, Y., et al., Comparison on photocatalytic degradation of gaseous formaldehyde by TiO_2, ZnO and their composite. Ceramics International. 38(6) (2012): 4437-4444.

[55] Kobayashi, T., H. Yoneyama, and H. Tamura, Role of Pt overlayers on TiO2 electrodes in enhancement of the rate of cathodic processes. Journal of The Electrochemical Society. 130(8) (1983): 1706-1711.

[56] Chen, J., et al., Photocatalyzed oxidation of alcohols and organochlorides in the presence of native $TiO_2$and metallized TiO_2suspensions. Part (I): photocatalytic activity and pH influence. Water Research. 33(3) (1999): 661-668.

[57] Pichat, P., M.-N. Mozzanega, and H. Courbon, Investigation of the mechanism of photocatalytic alcohol dehydrogenation over Pt/TiO_2 using poisons and labelled ethanol. J. Chem. Soc., Faraday Trans. 1. 83(3) (1987): 697-704.

[58] Kaise, M., et al., Photocatalytic reactions of acetic acid on platinum-loaded TiO_2: ESR evidence of radical intermediates in the photo-Kolbe reaction. J. Chem. Soc., Chem. Commun. (4) (1993): 395-396.

[59] Huebner, A.L. and H.N. Chu, Instability and breakup of charged liquid jets. J. Fluid Mech. 49(2) (1971): 361-372.

[60] Fong, H., I. Chun, and D.H. Reneker, Beaded nanofibers formed during electrospinning. Polymer. 40(16) (1999): 4585-4592.

[61] Park, S., et al., Effects of ZnO nanopowder dispersion on photocatalytic reactions for the removal of Ag^{+} ions from aqueous solution. Journal of Electroceramics. 22(1-3) (2009): 105-109.

[62] Bhattacharya, S., et al., Plasticization of Poly(vinylpyrrolidone) Thin Films under Ambient Humidity: Insight from Single-Molecule Tracer Diffusion Dynamics. The Journal of Physical Chemistry B. 117(25) (2013): 7771-7782.

[63] Chai, J.H. and Q.S. Wu, Electrospinning preparation and electrical and biological properties of ferrocene/poly(vinylpyrrolidone) composite nanofibers. Beilstein J Nanotechnol. 4 (2013): 189-97.

[64] Yang, H., S. Zhu, and N. Pan, Studying the mechanisms of titanium dioxide as ultraviolet-blocking additive for films and fabrics by an improved scheme. Journal of applied polymer science. 92(5) (2004): 3201-3210.

[65] Kharroubi, B., et al., Mn doping effect on the structural properties of ZnO-nanostructured films deposited by the ultrasonic spray pyrolysis method. Physica Scripta. 86(1) (2012): 015805.

[66] Hsu, S., Handbook of Instrumental Techniques for Analytical Chemistry. Chapter15 Infrared spectroscopy.

APPENDICES

APPENDIX A

THE Zn AND O2 MAPING OF PVP /ZnO FIBERS BEFORE IRRADIATION.

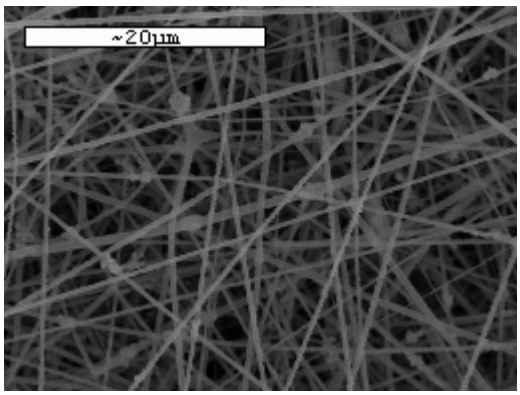

(a)

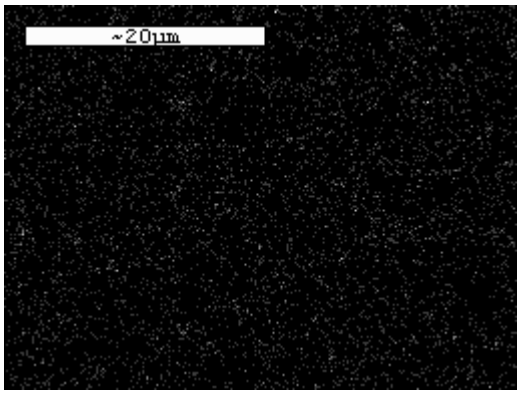

(b)

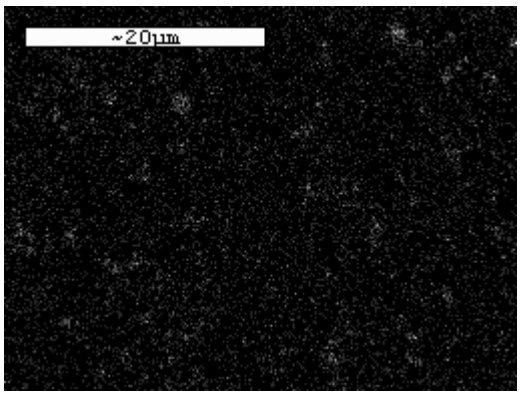

(c)

Fig.A.1 SEM image of PVP/ZnO fibers before irradiation a), the O_2 mapping b) and the Zn maping.

APPENDIX B

THE Zn AND O_2 MAPING OF PVP /ZnO FIBERS AFTER IRRADIATION.

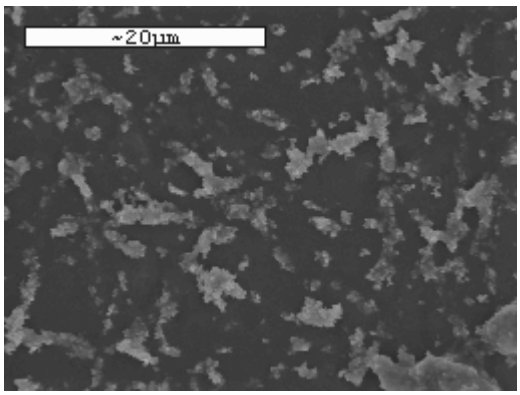

(a)

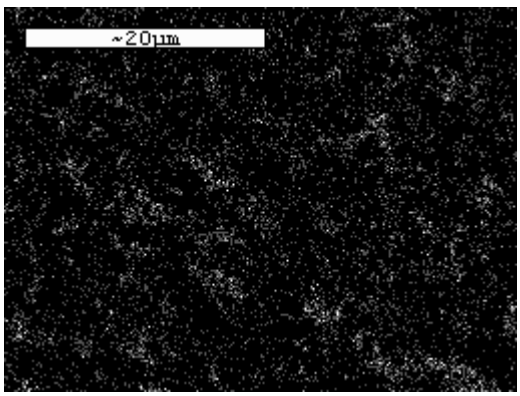

(b)

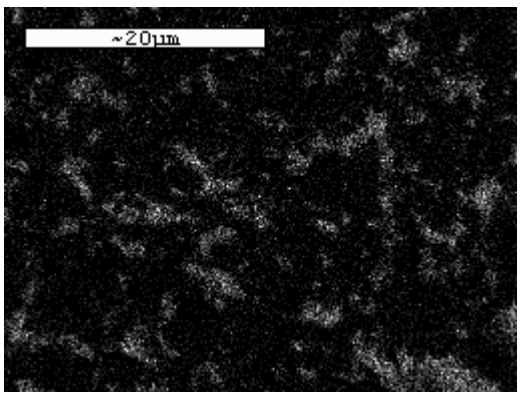

(c)

Fig.B.1 SEM image of PVP/ZnO fibers after 12 hr. irradiation a), the O_2 mapping b) and the Zn maping.

APPENDIX C

EFFECT OF APPLIED VOLTAGE ON THE SIZE AND AMOUNTS OF BEAD ON FIBERS

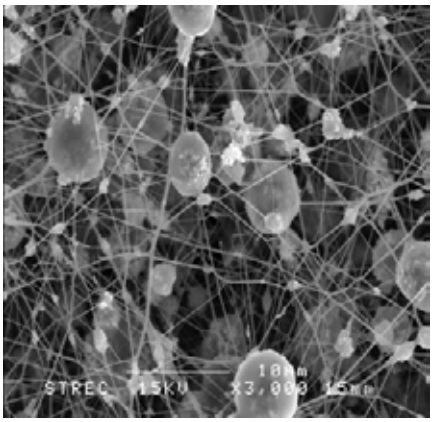

(a)

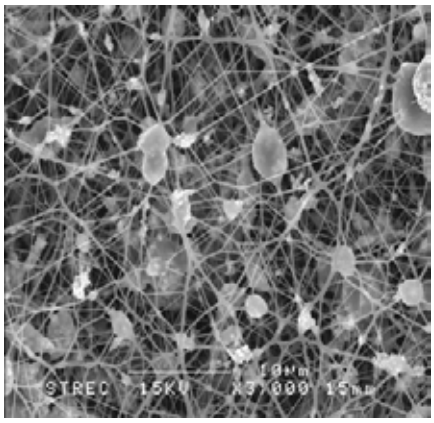

(b)

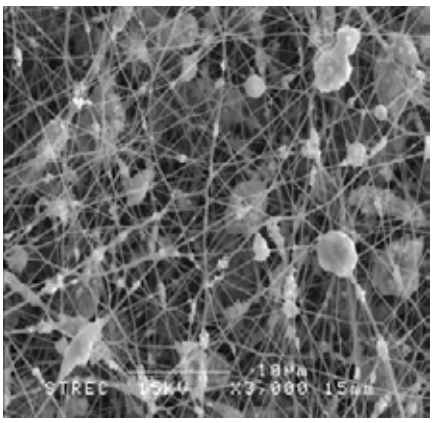

(c)

Fig.C.1 SEM micrographs of PVP nanofibers using 8wt% of PVP to Ethanal and varying applied voltage (a)13kV, (b)17kV, (c) 21kV.

APPENDIX D

LIST OF PUBLICATION

1. Nuchaporn Chewasatn, Varong Pavarajarn and Tawatchai Charinpanitkul, "Turnable fabrication of nanofibers polyvinyl pyrolydone – zinc oxide using electrospining method" , The 1st Joint Conference in Renewable Energy and Nanotechnology 2012, Bangkok, Thailand, November 19-20, 2012

2. Nuchaporn Chewasatn, Chompooptich Termvidchakorn,Varong Pavarajarn and Tawatchai Charinpanitkul, "Direct dispersion of ZnO nanoparticle in PVP fiber using electrospinning method", 10th Biomass-Asia Workshop, Bangkok, Thailand, August 5-6, 2013

VITA

Miss. Nuchaporn Chewasatn was born on 6th December, 1988, in Bangkok, Thailand. She received a graduated Bachelor's Degree of Science with the department of Chemical Technology from Chulalongkorn University. She continued to study in Master degree in Center of Excellence in Particle Technology at Department of Chemical Engineering, Faculty of Engineering, Chulalongkorn University.